MODELING, ANALYSIS, AND DESIGN OF A 10 KVA, 20 KHZ TRANSFORMER

by

Isaac Lynnwood Flory IV

Thesis submitted to the Faculty of the
Virginia Polytechnic Institute and State University
in partial fulfillment of the requirements for the degree of
Master of Science
in
Electrical Engineering

APPROVED

Krishnan Ramu, Chairman

Robert H. Miller

Dan Y. Chen

May, 1993

Blacksburg, Virginia

MODELING, ANALYSIS, AND DESIGN OF A 10 KVA, 20 KHZ TRANSFORMER

by

Isaac Lynnwood Flory IV

Krishnan Ramu, Chairman

Electrical Engineering

(ABSTRACT)

The design of a high-frequency transformer at levels above 1 kVA is limited by the winding and core materials which are available. This research presents methods for the design and modeling of a 10 kVA transformer operating at a frequency of 20 kHz using readily available materials.

A special winding technique is employed to increase both energy density and transformation efficiency by reducing leakage inductance and eddy current losses in the windings. The procedures for calculating the equivalent circuit parameters applicable to this design are outlined, and the calculated values compared with the measured quantities. A thermal analysis of the design is also explored using the equivalent circuit model as a basis for the calculation.

Some of the calculations are specific to this particular design, whereas others are quite generic, however the overall concepts employed in the design and analysis of this device have widespread application within the area of high-frequency, high-power transformer design.

Acknowledgements

I would first like to thank my committee chairman, Dr. Krishnan Ramu, for making this research possible and allowing me to participate even though my schedule did not allow for the keeping of regular hours on campus. His technical guidance throughout this research was invaluable, and my knowledge of the subject has been greatly augmented as a result of our association.

Many hours were spent in the laboratory both constructing and testing the prototypes for this design. I am indebted to Mr. Rajarshi Sen, who assisted greatly with this research by providing the circuitry necessary for testing the device, and also for being able to work when my schedule allowed. Thanks also go to my committee members, Dr. Dan Chen and Dr. Robert Miller, who were very patient regarding the delays which occurred just prior to the defense of this thesis, and who provided valuable suggestions regarding its content.

I would like to thank my employer, Hubbell Incorporated, for excusing me from legal obligation on this occasion and allowing me to perform this research. I am very grateful to my supervisor, Mr. Joe Nuckolls, Director of Advanced Engineering, for his overall support of my academic interests as well as the contributions of his technical expertise. The Vice-President of Engineering and Development for the Lighting Division, Mr. Lewis W. Kenyon, has also shown support all

during my graduate studies as has Mr. Edward Zamer, Industrial Relations Manager. I am also grateful to Mr. Ben Kaczmarek for his assistance in the preparation of the visual aids used in the defense of this research. Thanks also goes to the TDK Corporation of America, which provided core materials and technical information that were essential for the completion of this work.

I will always be grateful to my parents, Lynn and Nancy, for teaching me never to quit pursuing anything that I had begun.

Finally, I would like to thank my wife, Lisa, and my children, Carole and Zack, for their understanding and support over the past several years, during which my professional and academic agendas did not allow for an ideal family atmosphere. It is to them that this work is dedicated.

Table of Contents

List of Figures

List of Tables

Chapter 1

Introduction

1.1 Historical Review

Engineers have been designing transformers since the introduction of A.C. power distribution. Although there have been other methods developed to increase and decrease voltage and current levels, the transformer still remains the cornerstone of alternating energy conversion. In fact, the benefits of using A.C. power distribution virtually disappear without the existence of the transformer.

The field of power electronics employs transformers in various converter and regulator topologies. These methods of energy conversion have become quite popular since they offer greater energy processing capacity per unit volume and lower material cost than the older conventional technologies. As electrical products reduce in size, especially in the case of digital electronics, the greater energy conversion density is a key design requirement. This greater energy conversion density is attributable to higher operating frequencies which allow for a reduction in the size of the electromagnetic components.

In high power applications such as D.C. Power Transmission and Uninterruptable Power Supplies, the transformer is often used in conjunction with the D.C. to A.C. converter or

inverter stage. These inverters, which operate at relatively high frequencies, allow for a reduction in the physical size of the magnetics. As previously noted, this reduces the overall size and cost of the energy conversion stage.

The requirements for magnetic components used in power electronic designs is constantly changing due to advances in semiconductor technology. As the power handling and switching capabilities of the semiconductors increase, so do the requirements for higher power magnetics operating at higher and higher frequencies.

A vast amount has been written regarding transformers. Every text that I have read dealing with electromagnetic field theory, electric machinery, or network analysis addresses transformer operation to some extent, but in most cases the analysis does not include design or modeling information. Magnetoelectric Devices: Transducers, Transformers, and Machines by Gordon Slemon provides very useful insights into the transformer high-frequency model as well as methods for calculating the equivalent circuit parameters [2]. Another text by E.C. Snelling, Soft Ferrites: Properties and Applications, has become somewhat of a standard reference for high-frequency magnetics designers [11]. This text addresses every facet of the design and analysis procedures for many standard transformer and inductor configurations, and in some cases the principles used may be applied to various other core geometries. Electromagnetics by John D. Krauss, and Direct

and Alternating Currents by E.A. Loew are excellent electromagnetic references although they are in general more directed toward lower frequency applications [1,5].

Publications dealing with specific design procedures for transformers are somewhat limited. The Transformer and Inductor Design Handbook by William T. McLyman outlines specific procedures for various magnetic designs which makes it a popular reference for many designers [6]. This book also presents methods for estimating the thermal response of an electromagnetic device.

Many articles have been published dealing with various areas of high-frequency electromagnetic design pitfalls. An article by Audrey M. Urling, et. al. outlines the basic contents of several other related articles dealing with high-frequency winding losses [12]. Another article written by A.W. Lofti, et. al. of the Virginia Power Electronics Center offers interesting insights into the proximity effect, which are drawn on heavily by some of the calculations in this thesis [7].

1.2 Scope of Research Presented

As the applications for the transformer have broadened, certain operating challenges have arisen which unless addressed will tend to reduce the overall efficiency of the device. In high-frequency applications, losses due to eddy

currents in both the windings and the core create many problems leading to the success or failure of a design [6,11,12]. The engineer must also consider parameters such as leakage inductance and winding capacitance, which do not detract from the electrical efficiency, but do however hinder or distort the transfer of electrical energy.

To study the impact of these and other parameters upon the performance of a high-frequency transformer, the design and analysis of a high power inverter transformer was undertaken. The functional requirements for the transformer are:

Maximum Input Voltage - 350 Volts

Operating Frequency - 20 kHz

Maximum Apparent Power Capability - 10 kVA

Maximum Current Rise Time - 1.0 μs

It is the intent of this thesis to contribute methods for the analysis, development, and design of a 10 kVA, 20 kHz inverter transformer. Procedures for the experimental derivation of an equivalent transformer circuit are presented for the purpose of verifying the calculated circuit values. Finally, a simple thermal model is developed for the purpose of predicting the steady-state surface temperature at a particular dissipation level. The nomenclature used in this thesis is presented in Appendix A.

Chapter 2

Design of a 10 KVA, 20 Kilohertz Inverter Transformer

2.1 Electromagnetic Units of Measure

One of the complications encountered in electromagnetic design and analysis is organizing the design data and electromagnetic equations so that the units of measure are consistent. The IEEE has adopted the metric system of units which include, but are not limited to those listed in Table 2.1.

The confusion arises due to the fact that core and wire manufacturers do not agree upon which system of measurement is to be used. For instance, an American ferrite core manufacturer will often use the CGS or "Centigrade - Gram - Second" system of units when presenting their design data whereas a Japanese ferrite company will use the IEEE accepted RMKS or "Rationalized Meter - Kilogram - Second" system. In addition, wire manufacturers in the United States will almost always use the "English" system when describing their products. Data for converting from the English to the RMKS system of units is presented in Appendix B.

The same difficulties arise when studying electromagnetic texts and papers. Researching older publications, especially ones written in the United States, can lead to some confusion since the system of choice has changed over the years. This

Table 2.1. RMKS system of electromagnetic units and the permeability of free space.

Quantity	Symbol	Unit
Flux	Φ	Weber
Flux Density	B	Tesla
Magnetomotive Force	MMF	Ampere-Turn
Magnetic Intensity	H	$\frac{\text{Ampere-Turn}}{\text{Meter}}$
Permeability	μ	$\frac{\text{Henry}}{\text{Meter}}$
Length	l	Meter
Permeability of Free Space	μ_o	$4\pi * 10^{-7}$ H/m

in turn alters the appearance of the design equations which may lead to confusion. The experienced electromagnetic designer can recognize and translate between the different systems and associated equations with relative ease, however the designer who does not venture into electromagnetic design often can be misled by these inconsistencies.

2.2 Design Equations

Faraday's Law and Ampere's Law describe the electromagnetic relationships which dictate transformer operation. These relationships, coupled with the knowledge of how much current a conductor can safely carry and the dielectric strength of the materials being used provide the engineer with the necessary tools to design a transformer.

Faraday's Law states that the voltage induced in a coil of wire by a changing magnetic flux is:

$$V = -d\lambda/dt = -dN\Phi/dt = -N(d\Phi/dt) \qquad (2.1)$$

where λ represents the flux linkage of the coil which has flux Φ linking the N turns of the coil [3]. The flux density B can be substituted into Eq. 2.1 if the cross sectional area A is known:

$$\Phi = BA \qquad (2.2)$$

$$V = -N(dBA/dt) = -NA(dB/dt) \qquad (2.3)$$

Ampere's Law describes the relationship between the current within an enclosed path, and the magnetic field intensity H.

In its most basic form, which describes the magnetomotive force generated by N turns of a current I, Ampere's Law can be written as:

$$Hl = NI = MMF \tag{2.4}$$

where l is the length of the path in question. It is also a fact that the magnetic flux is related to the magnetomotive force by:

$$\Phi = MMF/R' \tag{2.5}$$

where R' is the reluctance of the material over which the MMF is being evaluated.

For the time-varying sinusoidal case, Eq. 2.2 can be written as:

$$\Phi = BA*SIN(2\pi ft) \tag{2.6}$$

where f is the excitation frequency. The time derivative of Eq. 2.6 yields a relationship which may be substituted into Eq. 2.1 giving the relationship:

$$V = 2\pi NABf \tag{2.7}$$

or in the root-mean-square form:

$$V_{rms} = 4.44NABf. \tag{2.8}$$

Eq. 2.8 is often referred to as the "transformer equation" due to its obvious application in transformer and inductor design [10].

The derivation of a similar relationship for a square-wave excitation is even more direct than that of the sinusoidal case. In its graphical form, Faraday's law can be written as:

$$V = N(\delta\Phi/\delta T)$$

The δT term may be considered the time period taken for the flux level to reduce to zero from the maximum value, reverse, and build to the opposite maximum value. It follows that this term is equal to one-half the period of the operating frequency. The change in flux, $\delta\Phi$, represents twice the maximum flux level which is generated over the flux swing as described above. As a result, Eq. 2.1 may be written as:

$$V = N(2\Phi/(1/2f)) = 4N\Phi f$$

which may be rewritten as:

$$V = 4NABf \tag{2.9}$$

Eq. 2.9 is the "transformer equation" which corresponds to a square-wave excitation.

2.3 Core Selection

Due to the 20 kHz operating frequency, conventional steel core use is out of the question, primarily due to the eddy current losses which would be encountered. These losses would both reduce the transformer's efficiency to an unacceptably low level as well as cause thermal difficulties.

Research in ferrite material technology began in the early part of the twentieth century with actual devices being developed as early as the 1940's [9]. Ferrites, which were originally termed "magnetic insulators", offer the transformer designer a core material with much lower eddy current losses than metallic cores for a given excitation. On the negative

side however, ferrites have lower saturation flux density levels than their metallic counterparts which does not make them as suitable for low frequency applications. For the frequency level of interest in this research, ferrite is the core material of choice.

Many companies all over the world manufacture ferrite cores which span a variety of geometries and operating characteristics. Unfortunately, the larger the physical size of core that is required, the fewer are the choices of core configurations and types of ferrite materials. The toroid configuration was chosen for this design because material was readily available. Table 2.2 lists selected mechanical and electrical specifications for the ferrite cores used in this design.

2.4 Winding Considerations

The first step in any magnetic design is the determination of the conductor size necessary to carry the full-load current. One need only know the current level desired and calculate the required conductor size based upon a current capacity of 750 to 1200 circular mils per amp for magnet wire [13]. This translates to 1062 to 1699 amperes per square inch or 1.6 to 2.6 amperes per square millimeter and applies when the wire is wound in the form of a multi-layer coil. However, this current carrying capacity increases

Table 2.2. Selected mechanical and electrical specifications for transformer core (toroid).

Quantity	Symbol	Value
Initial Permeability	μ_i	$2.639*10^{-3}$ H/m (±25%)
Curie Temperature	T_c	>200°C
Saturation Flux Density	B_s	0.5 T (@ 25°C)
Density	d	$4.8*10^{3}$ kg/m^3
Outer Diameter	**OD**	0.096 m
Inner Diameter	**ID**	0.075 m
Height	Ht.	0.030 m
Cross-Sectional Area	A_e	$3.134*10^{-4}$ m^2
Effective Core Length	l_e	0.2658 m

substantially if the wire is permitted to dissipate heat by increasing the spacings between adjacent turns.

2.4.1 Skin Effect

When passing current through a conductor at high frequencies a phenomena known as skin effect must be considered. In reviewing literature dealing with eddy current losses in conductors I have seen the skin effect described using several different methods, however all of the explanations represent different views of the same phenomena [2,4,6,7,11,12,13].

If a conductor is exposed to a time-varying magnetic field, eddy currents are induced which are detected as increased losses. The fields giving rise to these eddy currents are a result of currents in the vicinity of, or within the conductor itself. These eddy currents induced by internally generated magnetic fields give rise to the skin effect [11]. Fig. 2.1 shows the cross section of a wire with the main current I_1 flowing along the axis of the conductor. This alternating current gives rise to an alternating magnetic field H, which in turn gives rise to eddy currents I_e as shown. These eddy currents tend to oppose the main current in the vicinity at the axis and add to the current at the conductor surface. As the frequency increases, the effect becomes more pronounced for a given conductor size until all of the conducting area

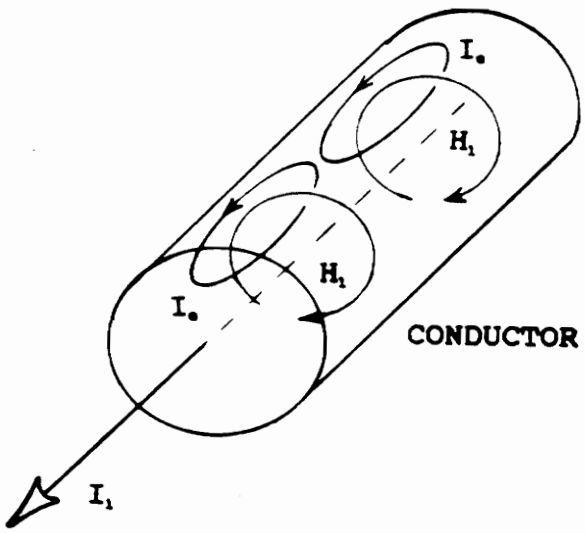

Figure 2.1. Eddy currents induced in a conductor due to internally generated magnetic field (skin effect).

can be considered as limited to a uniform depth at the surface. For the purposes of calculation, all of the current may be considered as passing through one skin depth on the periphery of the conductor [13]. The skin depth is equal to the depth required to attenuate an incident electromagnetic wave to 37% of its surface magnitude [11]. This value may be calculated using:

$$\delta = 0.066/\sqrt{f} \qquad (2.10)$$

where δ is the skin depth in meters and f is the operating frequency in hertz [13]. Calculation of an effective resistance R_{eff} can now be performed using the following relationship:

$$R_{eff}/R_{dc} \propto A_{dc}/A_{eff} \qquad (2.11)$$

where A_{eff} is the cross-sectional area of the conductor penetrated by one skin depth.

2.4.2 Proximity Effect

As mentioned in section 2.4.1, the magnetic fields which give rise to the eddy currents within a conductor may be generated within the conductor itself or from an external source. The magnetic fields contributed from external sources result in what is called the proximity effect [7,11]. The external sources are primarily other conductors in the same vicinity as the conductor being considered, which would be the case when examining a transformer winding. Fig. 2.2

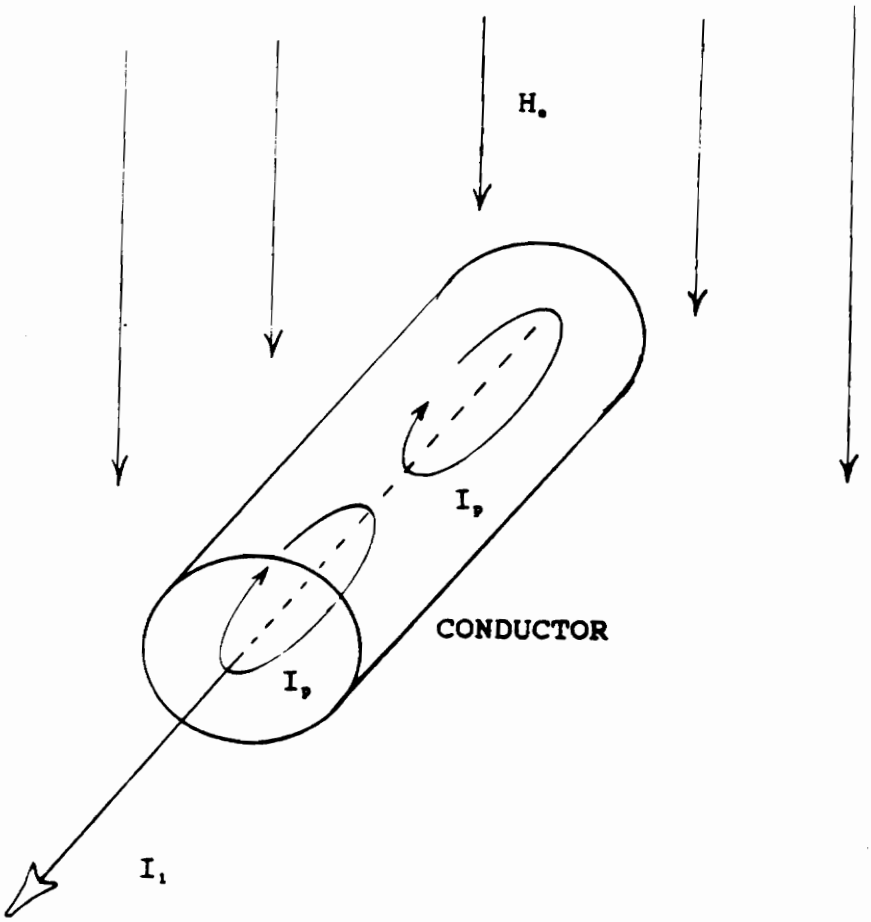

Figure 2.2. Eddy currents induced by and external time-varying magnetic field (proximity effect).

illustrates the cross-section of a conductor which is exposed to a time-varying magnetic field H_e. The eddy currents I_p induced in the wire tend to oppose current flow on one side of the conductor, but aid on the opposite side. The net result is a further reduction of effective conducting area beyond that of the skin effect. Unfortunately, the increase in resistance of a conductor due to proximity effect is not a conveniently estimated as is the case with the skin effect, especially when non-precision winding methods are used. For the purpose of estimating the reduction of conducting area due to proximity effects, it may be sufficient enough to know that conductors in close proximity which carry opposing currents tend to redistribute the area of conduction to the vicinity between the conductors as shown in Fig. 2.3a. Fig. 2.3b illustrates the tendency for adjacent conductors carrying current in the same direction to have their conducting areas redistributed to the areas farthest away from the adjacent conductor [7].

2.5 The Design Calculations

The most important items to be considered when designing a transformer of this type are electrical efficiency and thermal stability. Electrical efficiency and thermal performance are both controlled by limiting the power losses which consist of both winding and core losses. Factors which

Figure 2.3a. Effect of adjacent conductors upon current density distribution when currents are opposing.

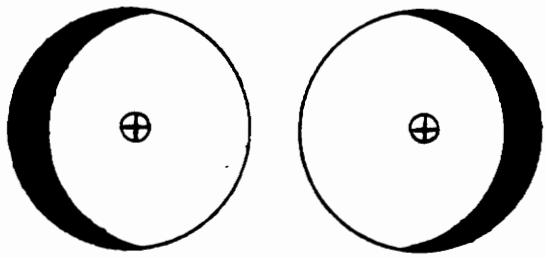

Figure 2.3b. Effect of adjacent conductors upon current density distribution when currents are coinciding.

appreciably add to the winding losses were discussed in section 2.4, and the core losses are a function of the operating frequency and the flux density level which is being generated within the core.

As stated in section 2.4, the first step in any transformer design is to determine the size of conductor required to carry the full-load current. From the electrical specifications provided in section 1.2, the maximum operating current level, assuming a unity power factor, is:

$$10 \text{ kVA} / 350 \text{ volts} = 28.57 \text{ amperes.}$$

For reasons of high-temperature performance and durability, the choice for the conductor was multi-stranded, 150°C insulated wire. Wire such as this can safely be operated at current density levels approaching 4500 amperes per square inch or equivalently 7 amperes per square millimeter. This result dictates that the minimum cross-section of conductor required to carry the full-load current is:

$$28.57 \text{ A} / (7 \text{ A/mm}^2) = 4.08 \text{ mm}^2$$

This result indicates that if this was a direct current, a minimum wire size of 11 AWG with a area of 4.168 mm^2 would be required. Wire of this size is however difficult to manipulate, and considering the skin effect, a single wire would not be the best choice. It would be advantageous to use multiple parallel wires resulting in a greater conductor surface area and therefore a more usable conductor cross-section. In addition, if multiple windings could be

intertwined or braided, the losses in the winding due to eddy currents could be further reduced [7,11]. The largest conductor available for this design with a temperature rating of over 100°C is 7 strand, 16 AWG, 150°C appliance wire. By using three 16 AWG wires in parallel, a cross sectional area of 3.93 mm^2 is achieved. Using three parallel wires also allows for regular braiding pattern which can be accomplished without the use of special equipment.

If the braided wire is now regarded as a single conductor, it is necessary to determine how many turns may be placed inside of the core window area. This may be facilitated by calculating an effective conductor radius which corresponds to the circumference required to encompass the three braided wires when they are equidistant from each other. The primary and secondary conductors each have an approximate effective radius RAD_{eff} of:

$$RAD_{eff} = 2.154r = 3.419*10^{-3} \text{ meters}$$

where r is the radius of a single 16 AWG wire, including the insulation. This gives an effective cross-sectional area of $3.673*10^{-5}$ square meters for each conductor. The window area of the core may be calculated from the data located in Table 2.2 yielding a value of $4.418*10^{-3}$ square meters. Allowing for a fill factor of 0.5 due to the random winding method, the maximum number of turns possible for this window area is:

(Window Area * 0.5)/Conductor Area = Total No. of Turns

$(4.418*10^{-3} m^2 * 0.5)/(3.673*10^{-5}) = 60.142 \approx 60$

A turns ratio of one was chosen for ease of analysis between the primary and secondary windings. This allows a maximum of 30 primary and 30 secondary turns within the transformer window area. Substituting the number of primary turns and the area of one core into Eq. 2.9 it is found that:

$$350 = 4*30*(3.134*10^{-4})*B*(20*10^{3})$$

therefore:

$$B = 0.465 \text{ Tesla}$$

which is unacceptably close to the saturation value of 0.5 Tesla. As the core temperature rises, the saturation flux density level drops, which would make 0.465 Tesla greater than the reduced saturation level. Since no more turns may be placed on the core, the only option is to increase the core cross-sectional area by stacking two cores together. This doubles the cross-section which reduces the flux density within the core by 50 percent for the same excitation.

In actuality, only 24 primary and 24 secondary turns were able to fit within the core window area, which is attributable to the braided conductors occupying a greater cross-section than originally calculated. It is therefore necessary to reduce the fill factor which will account for the spacing between the braided conductors themselves. This factor is easily obtained by dividing the actual number of turns achieved by the calculated number. A correction factor CF may be calculated as:

$$CF = \text{Actual Turns} / \text{Estimated Turns} = 0.8$$

and the new fill factor may be estimated by:

$$\text{Fill Factor} = 0.5 * CF = 0.4$$

Again using Eq. 2.9, the operating flux density may be recalculated:

$$350 = 4*24*(2*3.134*10^{-4})*B*(20*10^{3})$$

$$B = 0.29 \text{ Tesla}$$

which is well within the saturation flux density at core temperatures exceeding 120°C based upon the manufacturer's data.

This design's predicted overall performance will be based upon calculations presented in the chapters 4 and 5.

Chapter 3

The Transformer Equivalent Circuit

3.1 The Ideal Model

Virtually any general electrical engineering text explains elementary transformer operation using the equivalent circuit of Fig. 3.1 [1,2,3,4,5,6,9,10,14]. This equivalent circuit is used by educators to reenforce the concepts of turns ratio, reflected impedances and the dot convention. However, for modeling purposes, this circuit is quite inadequate and must be augmented by other equivalent circuit elements which help describe complete transformer operating characteristics over a range of frequencies.

3.2 Leakage Inductance

Leakage inductance refers to the reactance resulting from the lines of magnetic flux which are not coupled between the primary and secondary windings of a transformer [5,6]. In the design of a high-frequency transformer this parameter must be carefully considered to ensure that adequate power may be transferred from the primary to the secondary. If the leakage inductance is too great, the rise time will limit the amount current which is in phase with the driving voltage waveform, which dictates the amount of real power being transferred from

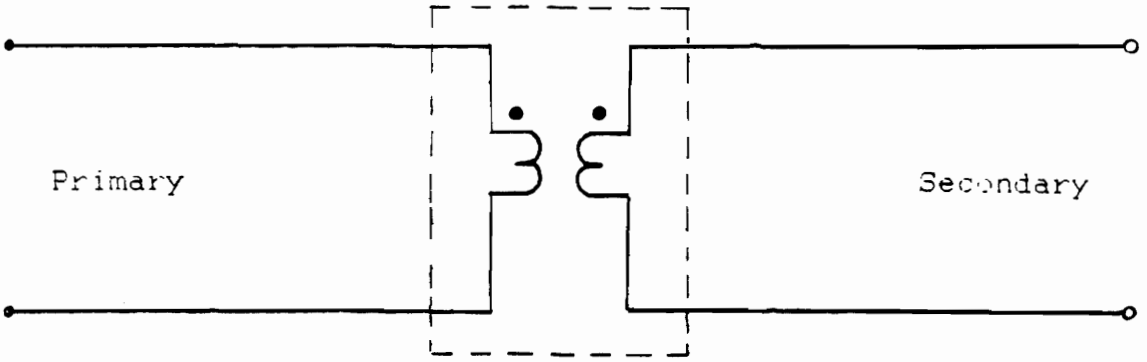

Figure 3.1. The ideal transformer model.

the primary to the secondary.

To reduce the amount of leakage, the primary and secondary windings may be interleaved [5,6,11]. This method is used primarily with precision winding techniques such as those used in the construction of transformers with shell or pot cores. For this particular toroidal design, since there are not any structured layers, the primary and secondary windings are intertwined or twisted together. Since the turns ratio for the device is one, the assembly of the transformer was accomplished by braiding separate primary and secondary conductors, twisting them together, and winding the entire bundle on the core.

3.3 Winding Resistance

As discussed in chapter 2, eddy current losses in the conductors at high frequencies can be modeled as increased winding resistance [11]. When incorporated into the model, these resistances provide a means of calculating the winding losses. For regular winding configurations, such as precision wound coils for shell or pot cores, there are equations and tables which can predict the effective resistance of a winding [11,12,16]. However, for the irregularly wound conductors which are being considered in this design, calculations will only serve as general approximations. A direct measurement of the effective winding resistance is the most accurate way

to determine these equivalent circuit elements.

3.4 Interwinding and Distributed Capacitance

There are two capacitive components which must be considered when describing high-frequency transformer operation, interwinding and distributed. All windings have a distributed or self-capacitance which may be visualized as a the capacitance between the turns of a winding and between the winding and its surroundings [11]. Minimizing this parameter may be achieved by using heavy wire insulations and winding methods which provide large turn to turn and layer to layer spacings.

The interwinding capacitance is determined by the proximity of the primary and secondary windings to each other, and the properties of the dielectric separating them. If the windings are greatly separated, the capacitance is low. However, as a result, the leakage inductance will be increased.

3.5 Magnetizing Inductance

As is the case with all magnetic core materials, an excitation current is required to magnetize the core and supply the hysteresis and eddy current losses [3]. The portion of this excitation current which contributes to the magnetization of the core material is referred to as the

magnetization current. This current lags the applied voltage by 90° and is therefore represented in the equivalent circuit as an inductance. The calculation of this equivalent inductance L_φ may be performed using the inductance equation:

$$L_\varphi = \mu N^2 A_c / l_c \qquad (3.1)$$

where N is the number of primary turns, μ is the permeability of the core material at the rated excitation voltage and frequency, and A_c and l_c are the core area and effective core length.

3.6 Core Loss

As mentioned in section 3.5, there is a component of the excitation current which corresponds to the core hysteresis and eddy current losses. This current, which is in phase with the excitation voltage, is called the core-loss current and is represented in the equivalent transformer model as a resistance [3]. The value of this resistance depends upon the core losses which are a function of the excitation frequency and flux density. Calculation of this parameter is performed using the equation:

$$R_c = V_p^2 / P_f \qquad (3.2)$$

where R_c is the core loss resistance, V_p is the applied primary voltage, and P_f is the core loss which is normally provided as part of the ferrite core data.

3.7 The High-Frequency Transformer Model

The equivalent circuit model for the high-frequency transformer is shown in Fig. 3.2. All of the circuit elements which were described in sections 3.2 through 3.6 are represented. The leakage inductances L_p and L_s, and the winding resistances R_p and R_s, are shown as series elements in both the primary and secondary windings respectively. The magnetizing inductance L_ϕ and core loss resistance R_c are placed in the model so that the excitation current does not pass from the primary to the secondary. Capacitors C_p and C_s are shown connected across the primary and secondary windings respectively, and C_{12}, the interwinding capacitance, is connected directly from the primary to the secondary.

3.8 The Calculated Model Parameters

3.8.1 Calculation of Leakage Inductance

Assuming that the window area of the core has been completely filled by the windings, the leakage inductance may be predicted by calculating the energy stored in the transformer windings. A reasonable estimation of the leakage inductance may be achieved by using the relationship:

$$0.5LI^2 = W \qquad (3.3)$$

where W is the energy stored in the windings. To make this

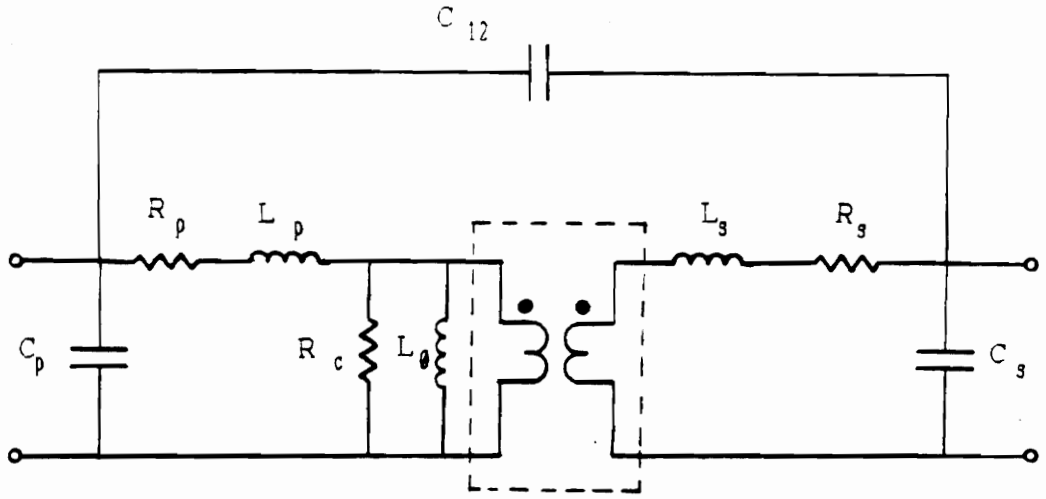

Figure 3.2. The high-frequency transformer model.

calculation however, the core and winding geometry must be known. If the core has a regular winding pattern and the window area of the core is rectangular, the calculation is rather straightforward [2]. However, if the windings of the transformer are placed on the core in a very random fashion, as is the case with the device being analyzed, some assumptions need to be made concerning the winding configuration.

What is known about the windings is that the conductors are made up of a set of three wires which are braided in a regular fashion. It is also known that the primary and secondary conductors are twisted together. What is not known is how the conductors are oriented within the core window area. Fig. 3.3 illustrates a toroidal core which has been, for the purposes of calculation, separated at a single location and unrolled. A magnetomotive force (MMF) diagram may be generated over the cross section of the winding if the configuration of the individual wires over the cross section is known. Unfortunately the exact location of these wires is unknown. However, if the winding orientation which gives the minimum MMF is combined with the orientation which gives the maximum MMF, then it is logical to assume that a median MMF distribution may be determined.

Fig. 3.4 depicts the cross-section of the twisted windings both in the minimum and maximum MMF generating positions. The wire insulation is taken into consideration since the spacings

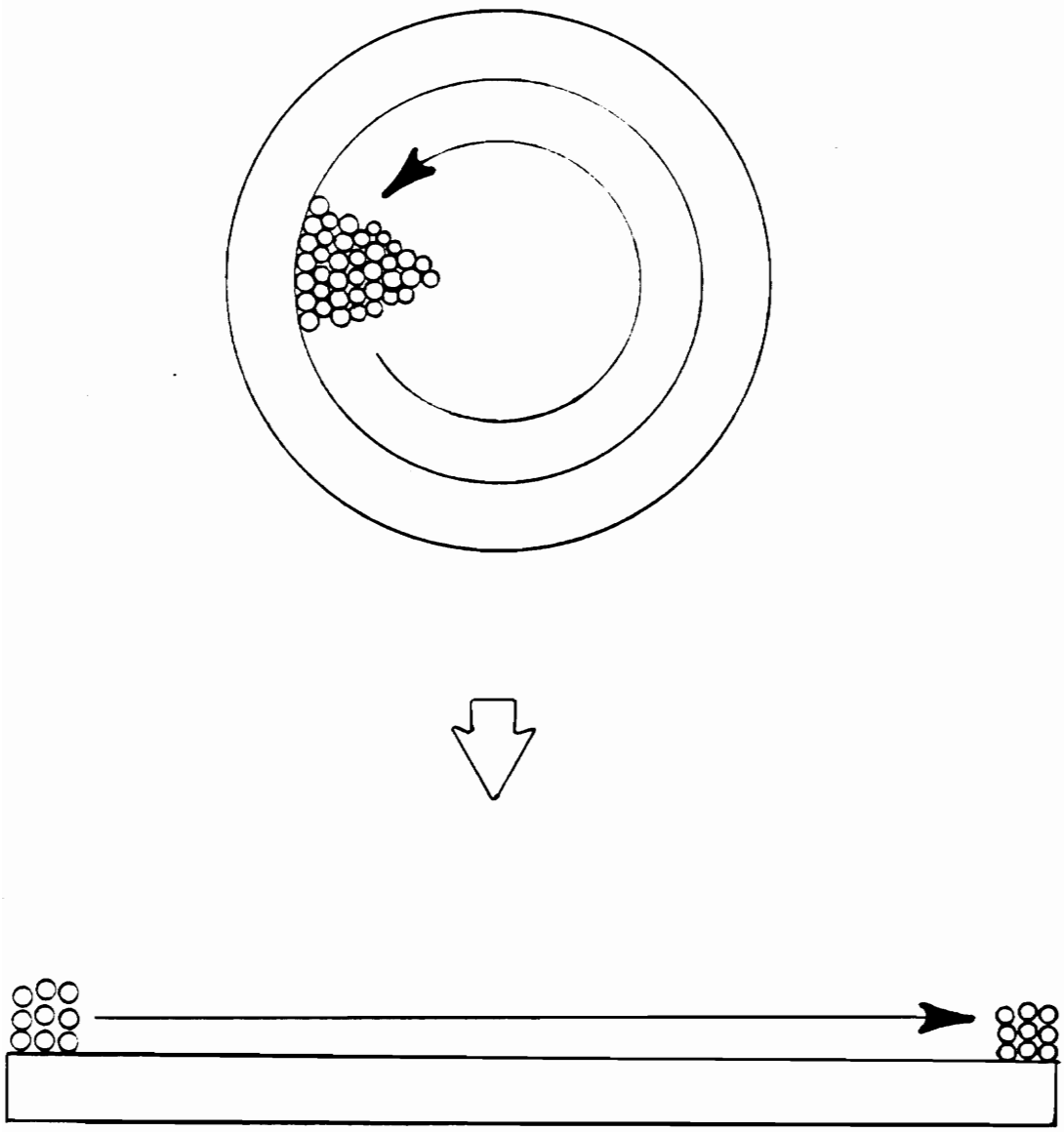

Figure 3.3. Toroidal core and windings configured for calculation of MMF distribution.

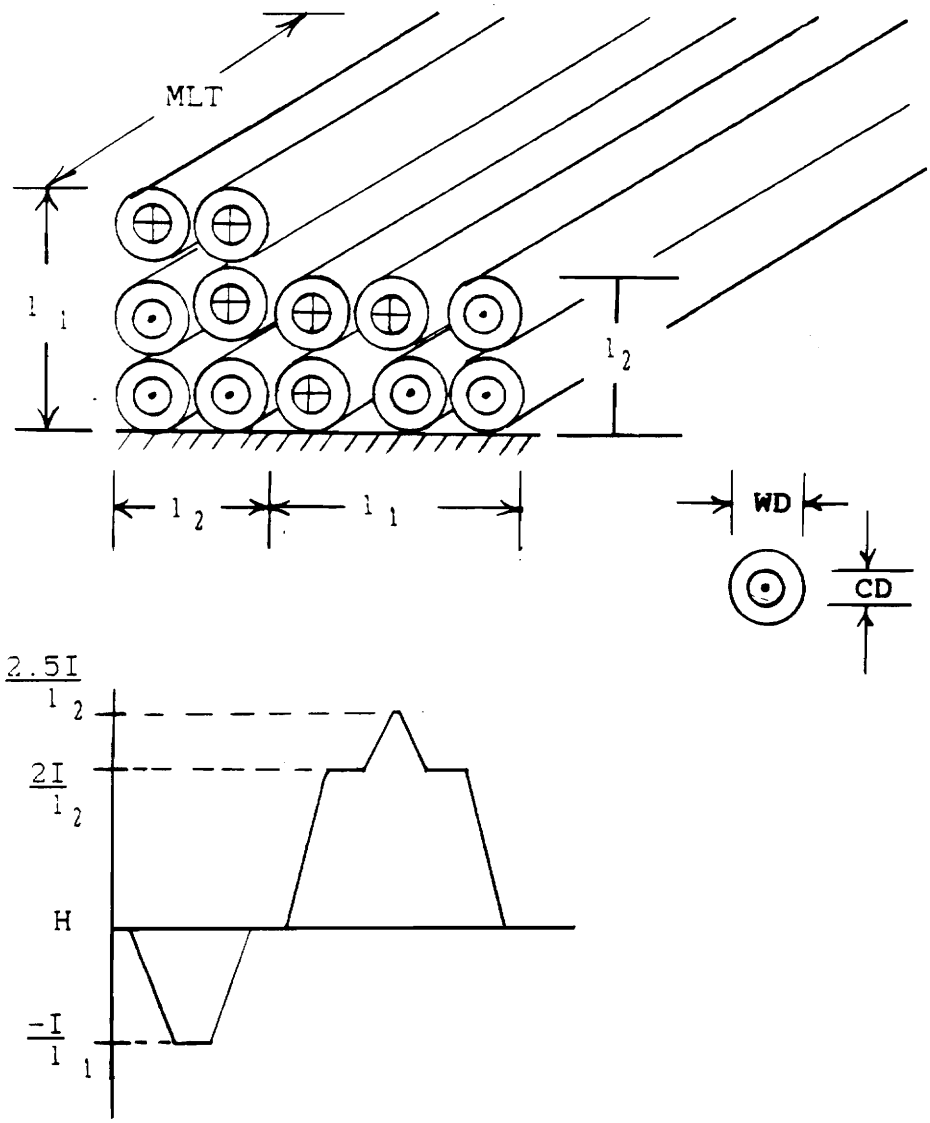

Figure 3.4. Winding configuration and MMF diagram.

which occur as a result of the insulation contribute substantially to the leakage of magnetic flux. The lower part of Fig. 3.4 shows the magnetic field diagram corresponding to the MMF distribution, and as can be seen, the magnetic field intensity varies greatly over the range of conductor orientations.

The energy stored in the windings may be calculated using the equation:

$$W = \frac{1}{2}\iiint B \cdot H \, dv$$

which may be represented as:

$$W = \frac{\mu_o}{2}\iiint H^2 \, dv \tag{3.4}$$

Using the magnetic field intensity diagram, the integral may be broken into two parts. The first part is the volume integral of H^2 from 0 to l_2 where the other two dimensions of the volume integral are the mean-length turn (MLT) of the winding and the vertical dimension l_1.

$$\frac{\mu_o}{2}\iiint H^2 \, dV = \frac{(MLT)(l_1)(\mu_o)}{2}\int_0^{l_2} H^2 dx \tag{3.5}$$

$$= \frac{(MLT)(l_2-WD)(\mu_o)(I^2)}{2(l_1)}$$

Performing a similar calculation from 0 to l_1, it is found that:

$$\frac{\mu_o}{2}\iiint H^2 \, dV = \frac{(MLT)(l_2)(\mu_o)}{2}\int_0^{l_1} H^2 dx \tag{3.6}$$

$$= \frac{(MLT)(\mu_o)(I^2)(10WD+2.25CD)}{2(l_2)}$$

Combining the results of Eqs. 3.5 and 3.6 it is determined that:

$$W_2 = (\mu_o)(I^2)(MLT)*[\ \frac{(l_2 - WD)}{2l_1} + \frac{(10WD + 2.25CD)}{2l_2}\ ] \quad (3.7)$$

where W_2 is the energy stored in two turns, and I is the current flowing through one wire of the braided conductor. It is estimated that the following are the physical quantities pertaining to Fig. 3.4:

$$WD = 3*10^{-3} \text{ meters}$$

$$CD = 1.29*10^{-3} \text{ meters}$$

$$l_1 = 10.5*10^{-3} \text{ meters}$$

$$l_2 = 7.2*10^{-3} \text{ meters}$$

$$MLT = 0.209 \text{ meters}$$

If these physical parameters are substituted into Eq. 3.7 it is found that:

$$W_2 = (6.526*10^{-7})I^2$$

Multiplying W_2 by 12 gives the total energy in the windings W_T:

$$W_T = 12 * W_2 = (7.832*10^{-6})I^2$$

This energy may be equated with the energy that would be stored in an equivalent inductance as shown in Eq. 3.3. The inductive current however is three times the current used in the previous calculations since each wire in the bundled conductor was considered separately, therefore:

$$0.5L(3I)^2 = (7.832*10^{-6})I^2$$

which leads to the result:

$$L = 1.740*10^{-6} \text{ henries}$$

This inductance represents the total inductance for both windings. Since the turns ratio is one, the inductance may be equally split between the primary and secondary windings giving:

$$L_p = L_s = 8.700*10^{-7} \text{ henries}$$

3.8.2 Calculation of Winding Resistance

As mentioned in section 3.3, the winding resistance at high-frequencies is a difficult parameter to calculate due to its dependence upon winding configuration and core geometry. Some publications provide tables and graphs which can aid in the prediction of this equivalent resistance, however there are many assumptions involved which include precision wound coils and uniform magnetic fields [11,12,16].

For the purpose of calculating the equivalent winding resistance, the following equation is proposed:

$$R_{HF} = R_{DC} * F_{SE} * F_{IPE} * F_{EPE} \qquad (3.8)$$

where R_{HF} is the equivalent high-frequency winding resistance, R_{DC} is the D.C. winding resistance, F_{SE} is a scaling factor due to the skin effect, and F_{IPE} and F_{EPE} are scaling factors due to internal and external proximity effects. The internal proximity effect is the increase in resistance due to the braiding process, and the external proximity effect is a further increase in resistance due to the primary and

secondary windings being twisted together.

The skin effect factor F_{SE} is easily determined knowing that the resistance of a conductor is directly proportional to its effective cross-sectional area. Therefore, the ratio of the DC cross-sectional area to the effective conductor cross-section due to the skin effect is the skin effect factor:

$$F_{SE} = A_{DC} / A_{SE} \tag{3.9}$$

The cross-sectional areas are easily determined as:

$$A_{DC} = \pi(0.5*CD)^2 \tag{3.10}$$

and:

$$A_{SE} = (\pi(0.5*CD)^2)-(\pi(0.5(CD-2\delta))^2) \tag{3.11}$$

where CD is the outer diameter of the conductor. After cancellation of terms, the following formula emerges:

$$F_{SE} = CD^2 / 4(\delta CD-\delta^2) \tag{3.12}$$

Substituting the operating frequency into Eq. 2.10, the skin depth δ is determined to be:

$$\delta = 0.066/\sqrt{(20*10^3)} = 4.67*10^{-4} \text{ meters}$$

The outer diameter of a 16 AWG conductor is $1.29*10^{-3}$ meters [6]. Substituting these values into Eq. 3.12 it is found that:

$$F_{SE} = 1.08$$

The internal proximity effect is illustrated in Fig. 3.5. The wires begin in a triangular orientation which, in a similar manner as that shown in Fig. 2.3b, illustrates that the effective conduction area has been decreased by approximately 67%. As the top wire passes between the other

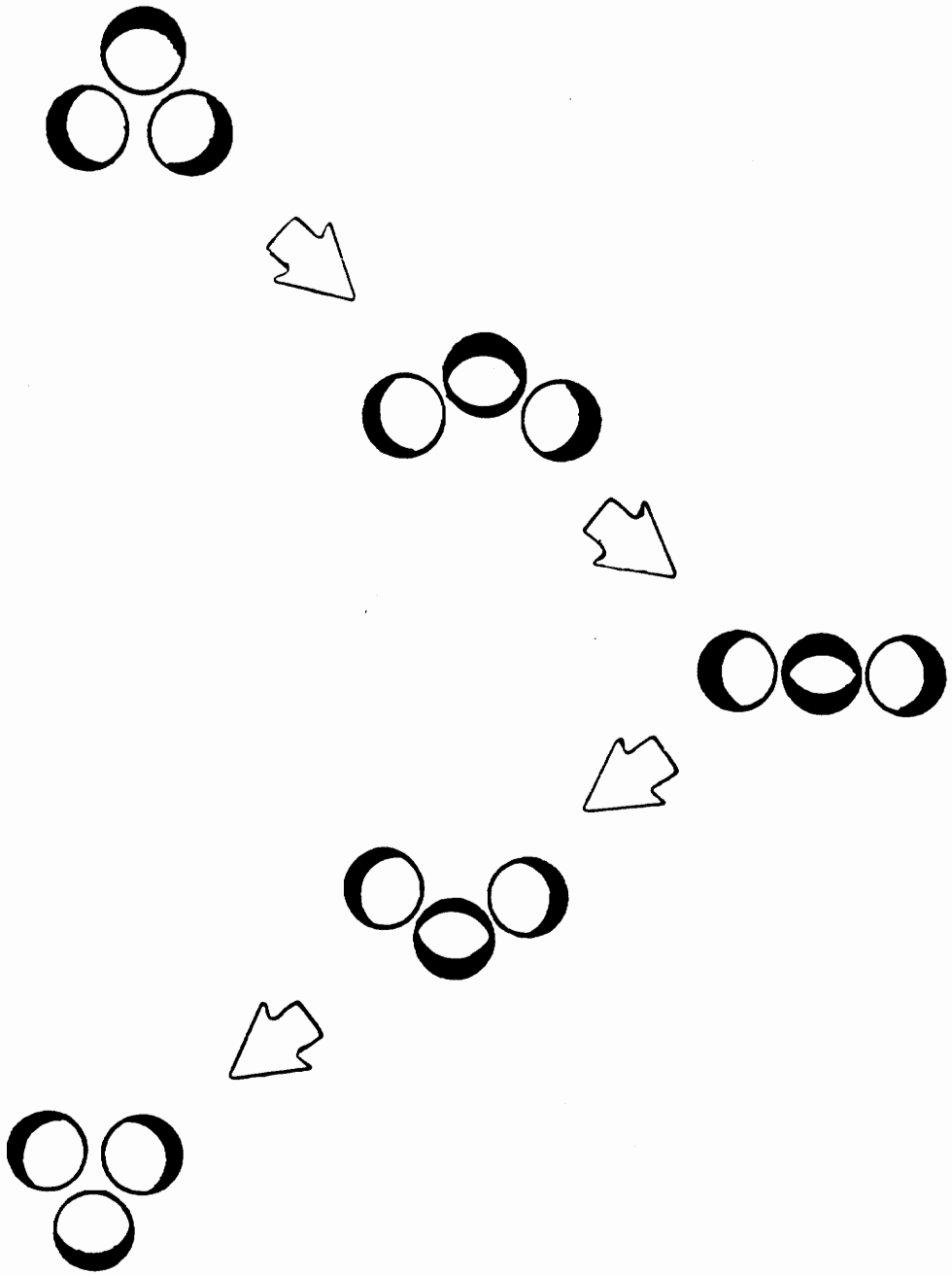

Figure 3.5. Effect of braiding (proximity effect) upon effective conductor cross-sectional area.

two wires, its effective conduction area increases due to cancellation of the magnetic fields generated by the outer two wires. A closer detail of the center wire is shown in Fig. 3.6. If the cross-section of this wire is viewed as a circle which contains an ellipse which again contains another smaller circle, the effective conduction area may be estimated.

The dashed circle in Fig. 3.6 is the area of infinite impedance and has already been taken into account by the skin effect factor F_{SE}. It is therefore necessary to calculate the further reduction in conduction area due to the ellipse. Eq. 3.11 describes the cross-sectional area of the conductor after taking the skin effect into account. A_E, the area of the ellipse minus the area of the non-conducting central circle is:

$$A_E = 0.25\pi(CD^2-2\delta CD) - 0.25\pi(CD-2\delta)^2 \qquad (3.13)$$

The percent reduction in cross-sectional area is therefore:

$$\% \text{ Reduction} = 1 - ((A_{SE} - A_E) / A_{SE})$$

Substituting Eqs. 3.11 and 3.13:

$$\% \text{ Reduction} = (0.5\delta CD-\delta^2) / (\delta CD-\delta^2) \qquad (3.14)$$

The two wires on either side of the center wire have also increased their effective conduction areas to approximately 50% of the area provided by the skin effect. As the three wires again achieve a triangular configuration, the effective cross-sectional areas return to their beginning values. One wire passing through the other two wires in this manner

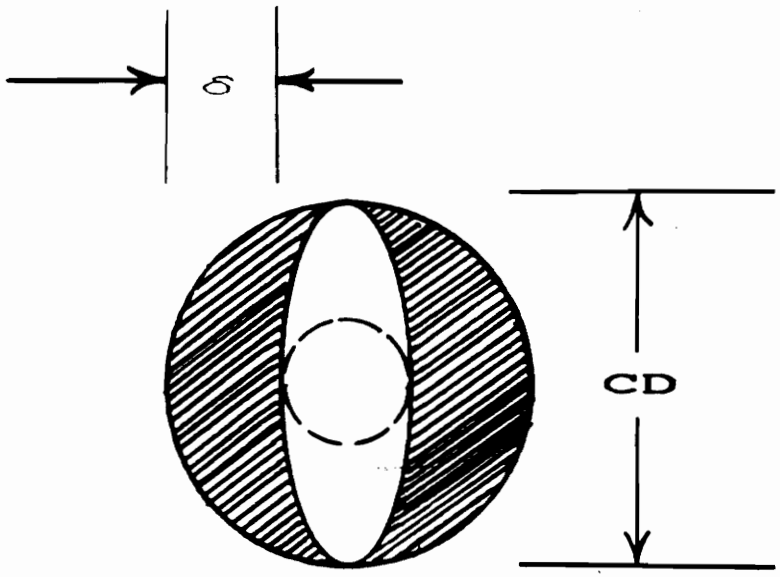

Figure 3.6. Center wire effective cross-section at point of minimum proximity effect due to outermost wires.

represents one third of a braid cycle. Substituting the physical parameters into Eq. 3.14, it is found that:

$$\% \text{ Reduction} = 21.63\ \%$$

Fig. 3.7 is a idealized plot of the effective conduction area of a single wire as a function of the braid cycle. This function may now be integrated to determine an average value which will be the inverse of F_{IPE}, the factor due to the internal proximity effect.

$$F_{IPE} = 0.463^{-1} = 2.16$$

Fig. 3.8 depicts the cross-section of the primary and secondary conductors at two different points during the twisting operation. These configurations reflect two of the infinite possibilities which may be created by the intermingling of the conductors. As a result of the proximity of one conductor to the other, there will be a further reduction of effective conductor cross-sectional area similar to that illustrated in Fig. 2.3a. At this point the estimation of this reduction in conductor area is quite speculative. In fact with the exception of F_{SE}, all of the factors which have been discussed in this section are graphical estimates. Upon inspection of Fig. 3.8, which suggests a possible redistribution of the effective conduction area, it is estimated that there is a further reduction of between 33 and 50 percent. Taking the inverse of an average of these conduction cross-sections it is found that:

$$F_{EPE} = ((0.67 + 0.5)/2)^{-1} = 1.71$$

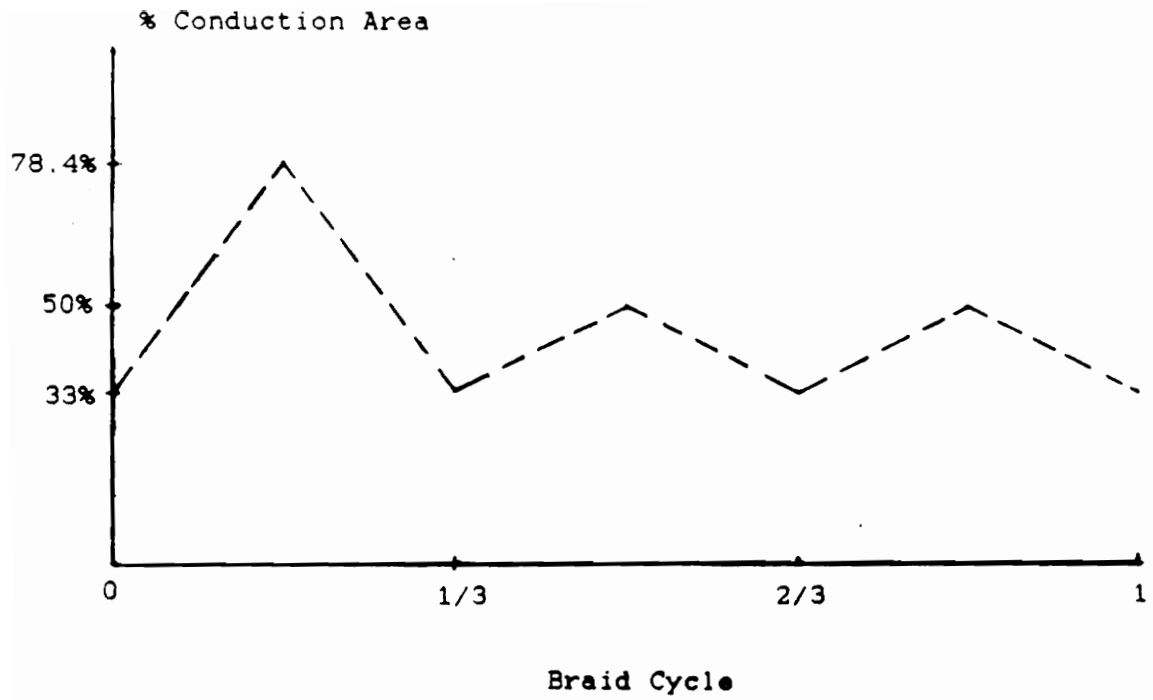

Figure 3.7. Estimated effective conduction area vs. braid cycle for a single wire.

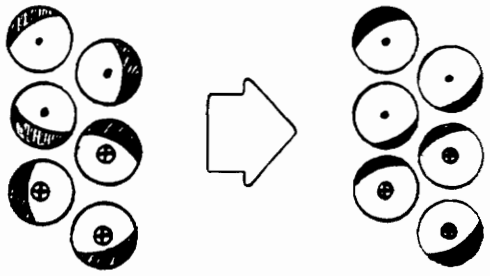

33% Reduction

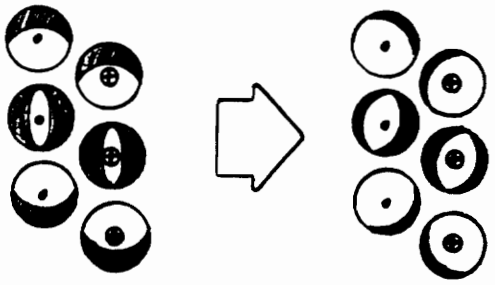

50% Reduction

Figure 3.8. Estimated redistribution of effective conduction area resulting from proximity of primary and secondary windings.

The primary and secondary conductors are each made of three, 16 AWG wires which are 6.528 meters in length. The DC resistance of 16 AWG is $131.8*10^{-6}$ Ω/cm ($131.8*10^{-4}$ Ω/m) [6]. The equivalent resistance of a winding is therefore:

$$R_{DC} = 6.528 * 131.8*10^{-4} / 3 = 2.868*10^{-2} \text{ ohms}$$

Substituting all of the values into Eq. 3.8 it is calculated that:

$$R_{AC} = R_p = R_s = 2.868*10^{-2} * 1.08*2.16*1.71 = 0.114 \text{ ohms}$$

3.8.3 Calculation of Interwinding and Distributed Capacitances

The interwinding capacitance may be calculated by using the equation:

$$C = \pi\epsilon_o L'/\cosh^{-1}(D/d) \qquad (3.15)$$

which is the capacitance between two parallel wires [17]. C is the capacitance in farads, ϵ_o is the permittivity of free space which is $8.854*10^{-12}$ farads per meter, L′ is the length of the windings before they are twisted together, D is the distance between the centers of the conductors, and d is the diameter of the conductor. Fig. 3.9 shows a cross section of the braided primary and secondary. These two conductors may be viewed as being single wires with centers that are in the middle of each triangular grouping. The measured distance between these centers is approximately 8mm or $8*10^{-3}$ meters. If the effective diameter of the conductor is taken to be the

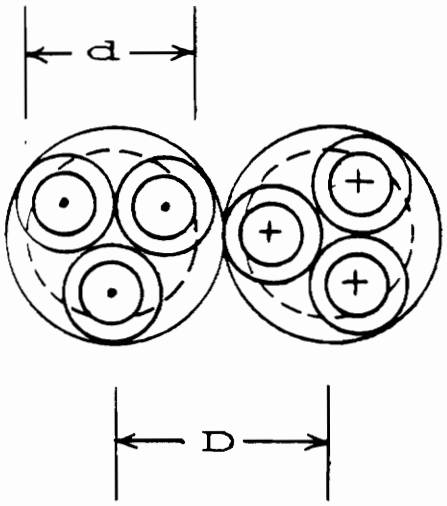

Figure 3.9. Primary and secondary conductor cross-section used for determining interwinding capacitance.

diameter of the dashed circle surrounding the conductor minus twice the insulation thickness it may be estimated that:

$$d = D - 0.8mm = 7.2*10^{-3} \text{ meters}$$

The length L′ corresponds to the length of a winding which is actually twisted together with the other winding. This twisting of the primary and secondary together reduces the overall length by 3.6%, which has been experimentally verified. It is known that the length of the twisted portion of the windings is 5.004 meters, therefore:

$$L' = 5.004 / (1-0.036) = 5.191 \text{ meters}$$

Substituting these values into Eq. 3.15 it is found that:

$$C = \pi(8.854*10^{-12})(5.191) / \cosh^{-1}((8*10^{-3})/(7.2*10^{-3}))$$

$$= 2.981*10^{-10} \text{ farads}$$

The distributed capacitance is usually determined by calculating all of the energy in the distributed capacitance and equating this value to $0.5CV^2$ [11]. This is analogous to the procedure used in section 3.8.1 to determine the leakage inductance. However, for this particular design, the distributed capacitance may be excluded from the equivalent circuit because of the winding technique used and the operating frequencies involved. If the windings would not have been twisted together and the adjacent turns of each winding been closer together, the distributed capacitance would have been larger which would therefore make the parameter more significant.

3.8.4 Calculation of the Magnetizing Inductance

To determine the magnetizing inductance for a specific design, the effective permeability at the rated excitation must be known. The flux density B may be determined easily from Eq. 2.8 or Eq. 2.9 if the primary voltage and frequency are known. The difficulty in determining the permeability is in determining the magnetic intensity H. Some core manufacturers provide hysteresis data at frequencies greater than the DC level, however most do not. The area within the hysteresis increases in a horizontal manner with increasing frequency which represents greater core losses. Therefore the permeability for a given flux density level decreases with increasing frequency. Without an idea of the hysteresis dimensions at the rated frequency, the magnetizing force and therefore the magnetizing intensity cannot be determined. Once this value of H is known however, the effective permeability may be calculated and Eq. 3.1 may be used to determine the value of the magnetizing inductance.

3.8.5 Calculation of the Core Loss Resistance

This parameter is easily found by calculating the flux density, determining the losses at that flux density, and using Eq. 3.2. For the purposes of testing, the excitation voltage used was 200 volts. The flux density may be

determined using Eq. 2.9:

$$200 = 4(24)(2*3.134*10^{-4})(20*10^{3})B$$

therefore:

$$B = 0.166 \text{ Tesla}$$

The loss curves, which are presented in Fig. 3.10, are now used to determine the watts loss per kilogram for the calculated flux density. Fig. 3.10 indicates that the losses are approximately 20 watts per kilogram for this excitation. This value is used to determine the total losses for the core:

$$P_r = 20 \text{ watts/kg} * 0.8 \text{ kg} = 16 \text{ watts}$$

The core loss resistance may now be calculated using Eq. 3.2:

$$R_c = (200 \text{ volts})^2 / 16 \text{ watts} = 2500 \text{ ohms}$$

3.9 Measured Values

3.9.1 The Short-Circuit Test

The short-circuit test is commonly used to determine the winding resistance and leakage inductance of a transformer. Fig. 3.11 shows the equivalent circuit of a transformer that has a turns ratio of one and no distributed capacitances. If terminals 3 and 4 are shorted together, and if R_c and L_ϕ are removed due to their large magnitudes, the equivalent circuit illustrated in Fig. 3.12 remains. An analysis of the circuit of Fig. 3.12 using the data from the short-circuit test will reveal the equivalent circuit parameters R_p, R_s, L_p, and L_s.

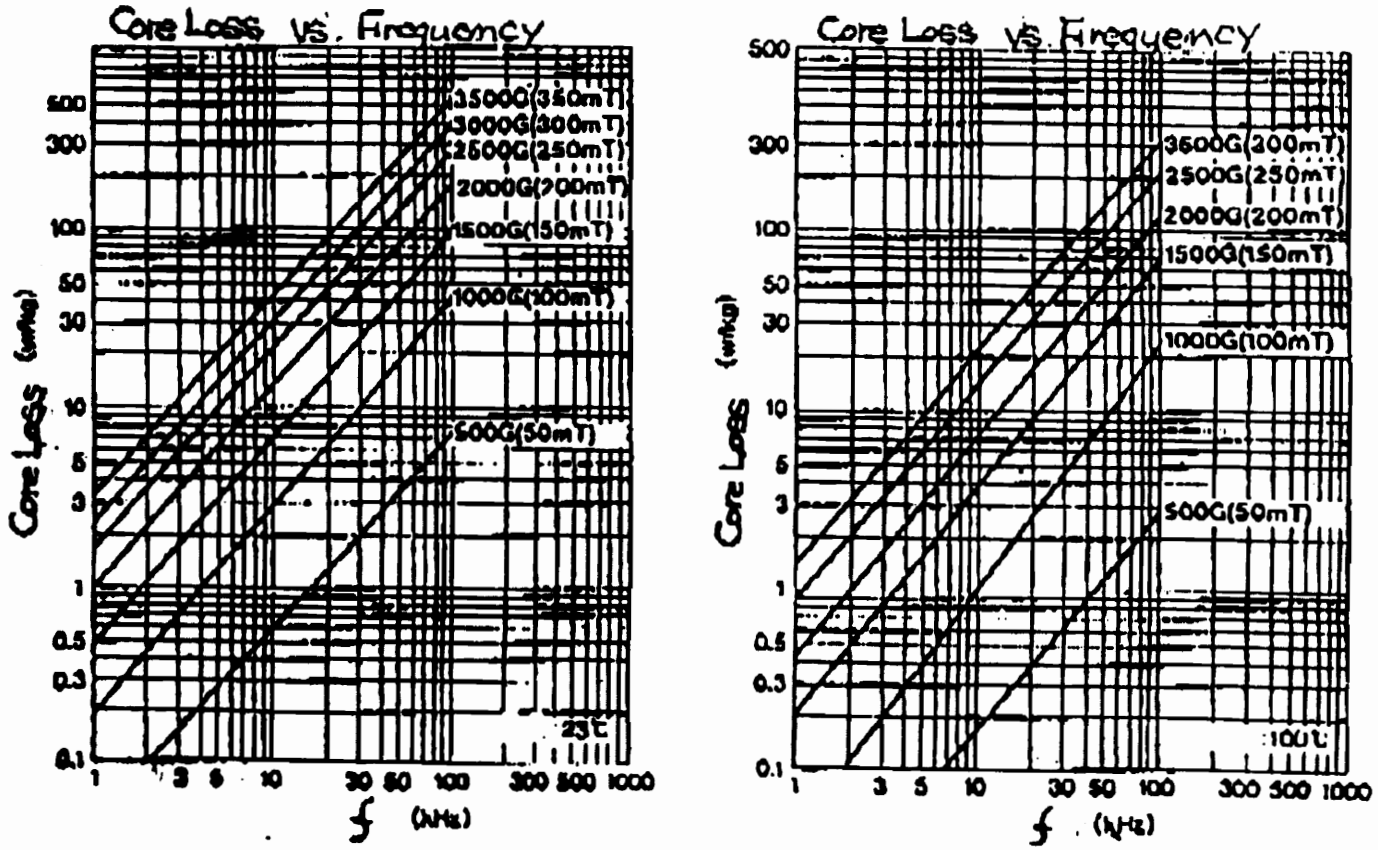

Figure 3.10. Loss curves for ferrite material (TDK PE-1).

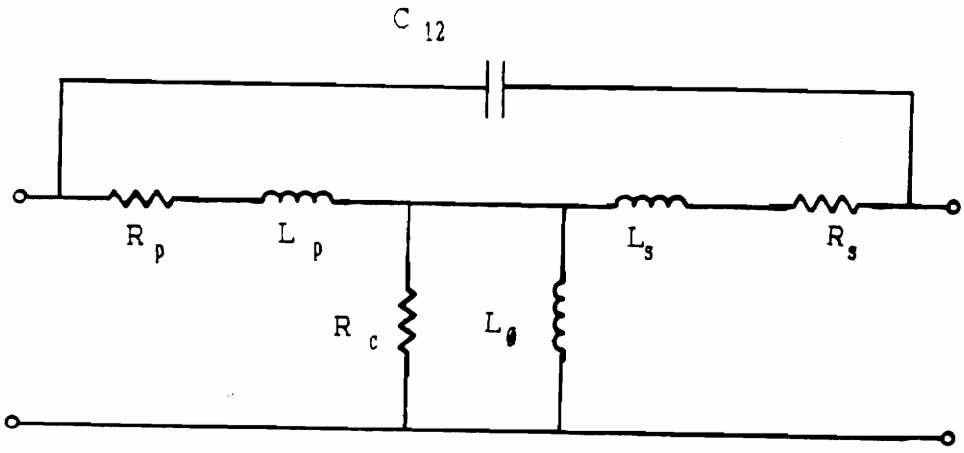

Figure 3.11. Equivalent circuit of transformer with a turns ratio of one, and no distributed capacitances.

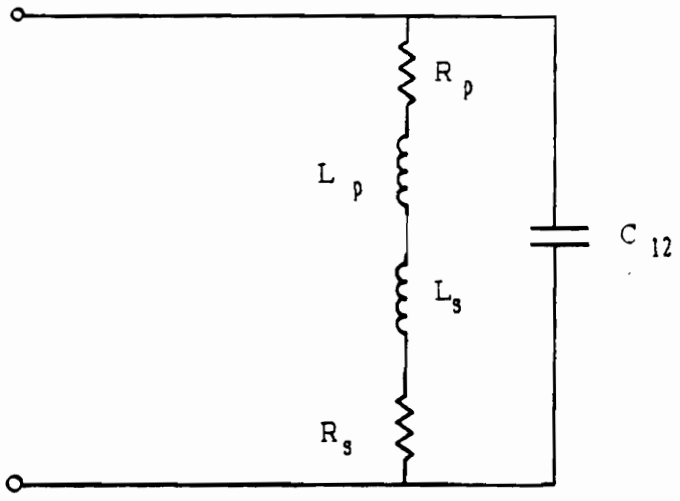

Figure 3.12. Approximate equivalent circuit of transformer under short-circuit conditions.

Analysis of the equivalent circuit of Fig. 3.12 is performed using the fundamental components of the applied voltage and resulting current. The behavior of the higher order harmonics may then be studied using the fundamental parameters [2]. The short-circuit voltage and current waveforms are shown in Fig. 3.13. Fourier coefficients for both waveforms were determined by manually sampling each waveform every $1*10^{-6}$ seconds for a period of $50*10^{-6}$ seconds, and using MATLAB software to perform a fast Fourier transform. The fundamental coefficients were determined from this analysis resulting in the following fundamental waveforms:

$$V_{fund} = 3.0799\cos(1.26*10^5*t)+4.0857\sin(1.26*10^5*t) \text{ volts}$$

$$I_{fund} = -4.7430\cos(1.26*10^5*t)+12.7665\sin(1.26*10^5*t) \text{ amperes}$$

which in phasor form are:

$$V_{fund} = 5.1165\cos((1.26*10^5*t)-0.9249) \text{ volts}$$

$$I_{fund} = 13.6191\cos((1.26*10^5*t)-1.9265) \text{ amperes}$$

Dividing the fundamental voltage vectorally by the fundamental current gives the fundamental impedance:

$$V_{fund} / I_{fund} = Z_{fund} = 0.3757 \underline{/1.0017} \text{ ohms}$$

or equivalently in complex form:

$$Z_{fund} = 0.2025 + j2.51*10^{-6} \text{ ohms}$$

The interwinding capacitance, easily measured using a digital impedance bridge, is determined to be $2.99*10^{-10}$ farads. Knowing this capacitance only leaves the winding resistances and leakage inductances as unknowns. These parameters may be combined into one equivalent resistance and

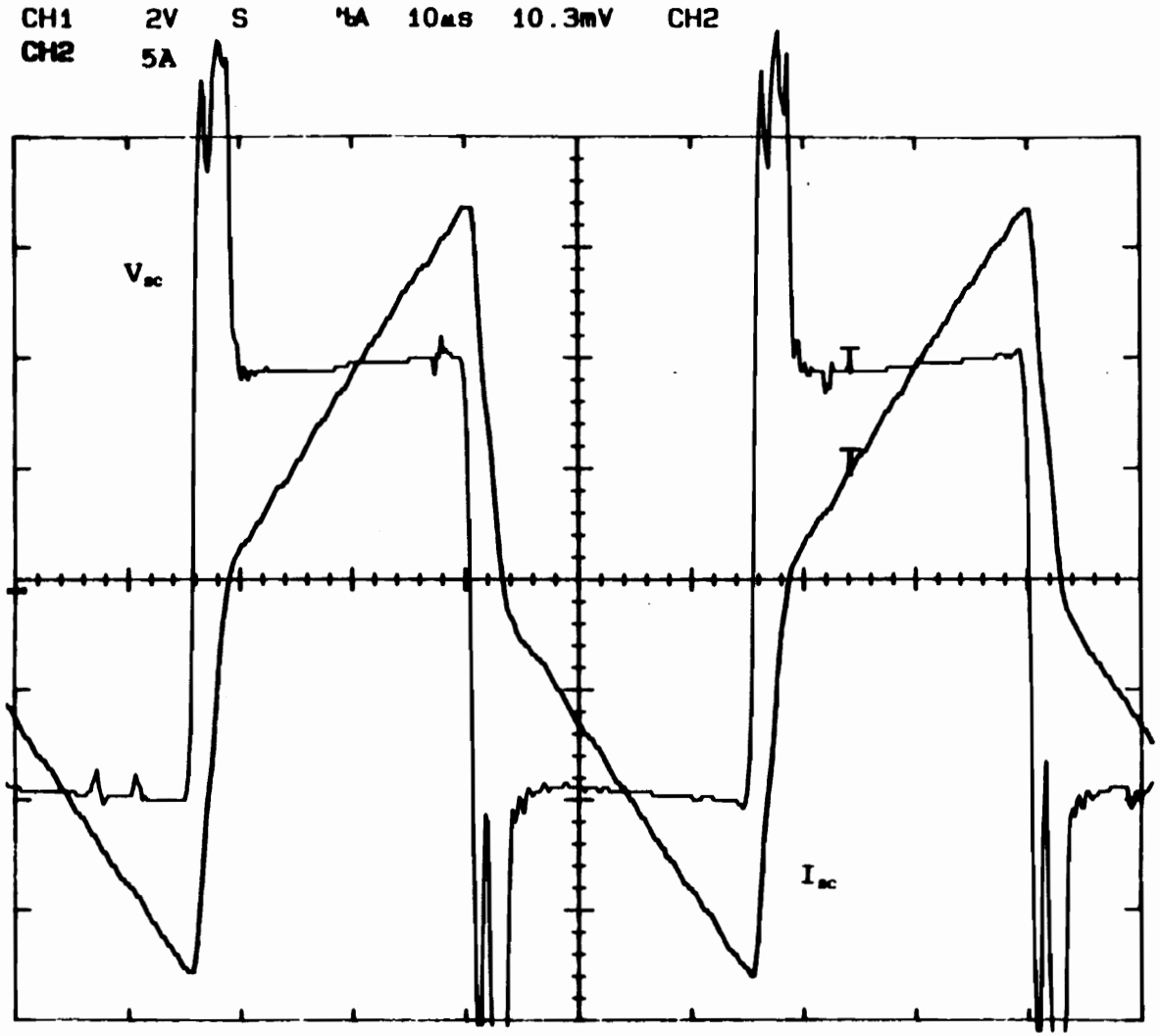

Figure 3.13. Input voltage and current waveforms under short-circuit conditions.

one equivalent inductance which reduces the number of unknowns to two. The fundamental impedance represents a magnitude and an angle which provides the solutions to two independent equations based upon the circuit of Fig 3.12. These equations are:

$$0.3757 := \sqrt{\left[\frac{R_T^2 + \left[w^2 L_T^2\right]}{1 + \left[\left[w R_T C_{12}\right]^2\right] + \left[\left[w^2 L_T C_{12}\right]^2\right]}\right]}$$

$$1.0017 := -\operatorname{atan}\left[\left[-w\frac{L_T}{R_T}\right] + \left[\left[w C_{12}\right]\frac{\sqrt{R_T^2 + \left[w^2 L_T^2\right]}}{\cos\left[\operatorname{atan}\left[-w\frac{L_T}{R_T}\right]\right]}\right]\right]$$

where R_T is the total resistance, L_T is the total inductance and w is the frequency in radians per second. The solutions of these two simultaneous equations were determined using MATHCAD to be:

$$R_T = 0.202454 \text{ ohms}$$

$$L_T = 2.508342*10^{-6} \text{ henries}$$

Since this transformer has a turns ratio of one:

$$R_p = R_s = 0.101227 \text{ ohms}$$

$$L_p = L_s = 1.254171*10^{-6} \text{ henries}$$

3.9.2 The Open-Circuit Test

If terminals 3 and 4 are left open in Fig. 3.11, then all

of the current which flows as a result of a primary voltage will pass through either the core loss resistance R_c or the magnetizing inductance L_φ. If Fig. 3.11 is redrawn as shown in Fig. 3.14a, and all of the other equivalent circuit elements have already been determined, then the calculation of R_c and L_φ may be accomplished.

Using MATLAB, the fundamental components of the primary voltage and current waveforms recorded during the open-circuit test were determined to be:

$$V_{fund} = -16.0539\cos(1.26*10^5*t)-292.258\sin(1.26*10^5*t) \text{ volts}$$

$$I_{fund} = 0.8589\cos(1.26*10^5*t)-0.17553\sin(1.26*10^5*t) \text{ amperes}$$

which in phasor form are:

$$V_{fund} = 292.699\cos((1.26*10^5*t)+1.6256) \text{ volts}$$

$$I_{fund} = 0.8766\cos((1.26*10^5*t)+0.2016) \text{ amperes}$$

The equivalent fundamental impedance is therefore:

$$V_{fund} / I_{fund} = Z_{fund} = 333.897 \angle 1.4241 \text{ ohms}$$

or equivalently in complex form:

$$Z_{fund} = 48.813 + j330.31 \text{ ohms}$$

Referring back to section 3.8.4, it was stated that the magnetic intensity H was necessary in determining the effective permeability μ so that the magnetizing inductance could be calculated. The open-circuit test has revealed the correct values of B and H required for this calculation. Using the fundamental sinusoidal components of the open-circuit current and voltage, the flux density B and magnetic intensity H may be determined using Eqs. 2.4 and 2.8:

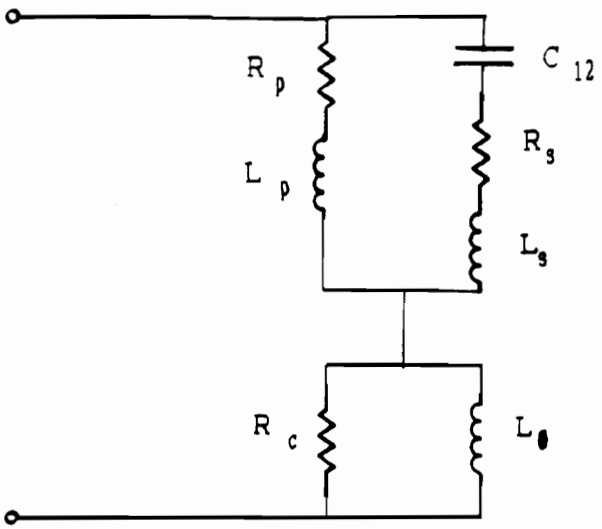

Figure 3.14a. Equivalent circuit of transformer under open-circuit conditions.

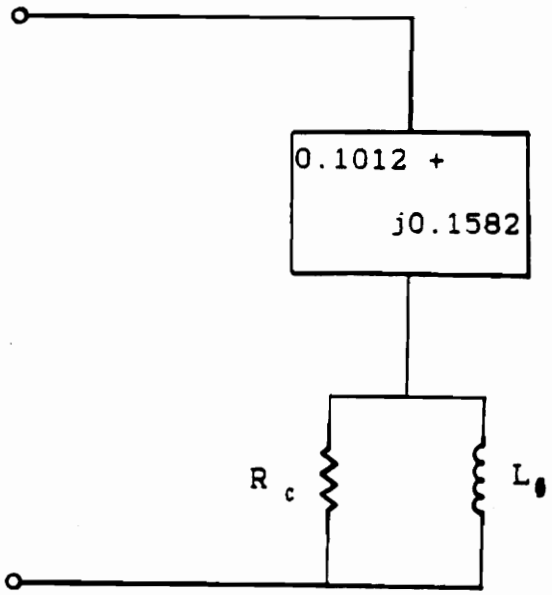

Figure 3.14b. Equivalent circuit of transformer under open-circuit conditions with impedance determined from the short-circuit test.

$H = (24*0.8766)/0.2658 = 79.15$ amperes/meter

$B = 292.699/(\sqrt{2}*4.44*0.6268*10^{-3}*24*20000) = 0.154$ Tesla

The effective permeability if found to be:

$$\mu = B/H = 0.154/79.15 = 1.951*10^{-3} \text{ henries/meter}$$

Eq. 3.1 is now used to determine the magnetizing inductance:

$$L_\varphi = (1.951*10^{-3} * 24^2 * 0.6268*10^{-3})/0.2658$$

$$= 2.650*10^{-3} \text{ henries}$$

If the known elements in Fig. 3.14a are combined into a net impedance as shown in Fig. 3.14b, then a real impedance equation and an imaginary impedance equation may be written and equated to the real and imaginary components of Z_{fund}. These equations are:

$$48.813 := 0.1012 + \left[\left[\frac{w \cdot R_C \cdot L_\Phi}{\sqrt{R_C^2 + [w \cdot L_\Phi]^2}}\right] \cdot \left[\cos\left[1.57 - \operatorname{atan}\left[w \cdot \frac{L_\Phi}{R_C}\right]\right]\right]\right]$$

$$330.31 := 0.1582 + \left[\left[\frac{w \cdot R_C \cdot L_\Phi}{\sqrt{R_C^2 + [w \cdot L_\Phi]^2}}\right] \cdot \left[\sin\left[1.57 - \operatorname{atan}\left[w \cdot \frac{L_\Phi}{R_C}\right]\right]\right]\right]$$

Again, using MATHCAD software, the solutions of these equations were found to be:

$$R_c = 2298.76 \text{ ohms}$$

$$L_\varphi = 2.673*10^{-3} \text{ henries}$$

The calculated and measured high-frequency models of the

transformer are shown in Figs. 3.15a and 3.15b.

The errors between the measured and calculated equivalent circuit parameters may now be found:

L_p and L_s error = $(1.254*10^{-6} - 0.87*10^{-6})/1.254*10^{-6}$

= 30.6%

R_p and R_s error = $(0.114 - 0.1012)/0.1012$ = 12.6%

C_{12} error = $(2.99*10^{-10} - 2.981*10^{-10})/2.99*10^{-10}$

= 0.3%

L_φ error = $(2.673*10^{-3} - 2.65*10^{-3})/2.673*10^{-3}$ = 0.9%

R_c error = $(2500 - 2298.76)/2298.76$ = 8.8%

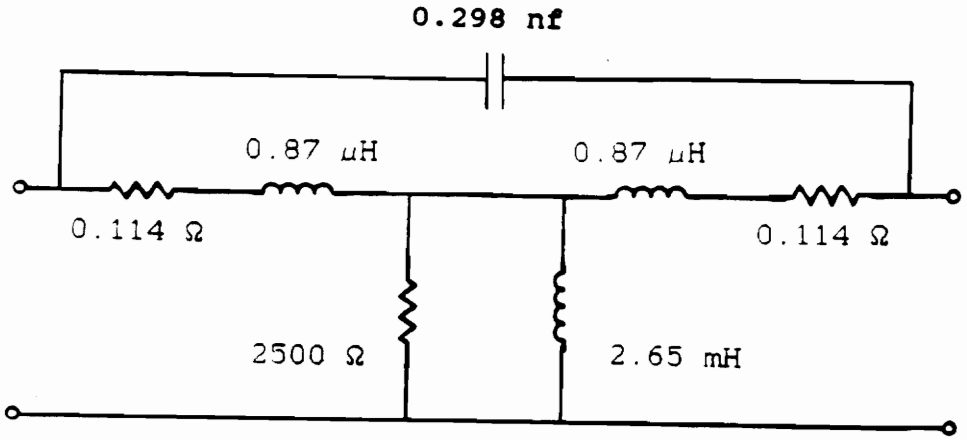

Figure 3.15a. Calculated equivalent transformer model.

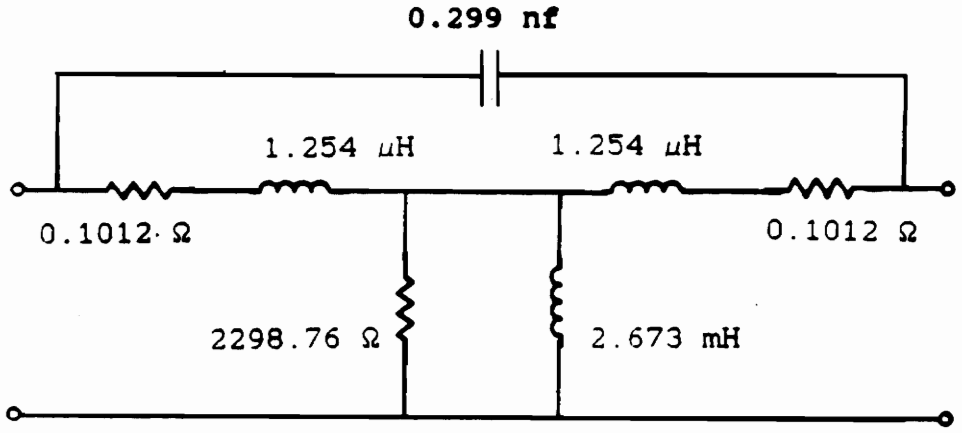

Figure 3.15b. Measured equivalent transformer model.

Chapter 4

The Operating Characteristics

4.1 Operating Data

The set-up used for functionally testing the transformer is illustrated in Fig. 4.1. Due to limitations of both the load resistance and the inverter, all data in this section was recorded with a primary voltage of approximately 200 volts and a load current of approximately 25 amperes resulting in an apparent power of 5 KVA. The purpose of these tests were to first verify that the transformer functioned within the measurable operating specifications outlined in section 2.5, and second to obtain data which could be used to verify the performance of the fundamental equivalent circuit of Fig. 3.15b.

Fig. 4.2 shows the primary operating voltage and current under the test conditions of Fig. 4.1. As can be seen, the voltage is not purely trapezoidal which is due to the switching characteristics of the inverter. Both of the waveforms were multiplied together giving the instantaneous power waveform which is shown in Fig. 4.3. To determine the input power delivered to the transformer, the positive volt-ampere portion of the waveform was integrated over one period resulting in the net energy per cycle. This energy was then multiplied by the operating frequency of the driving waveform

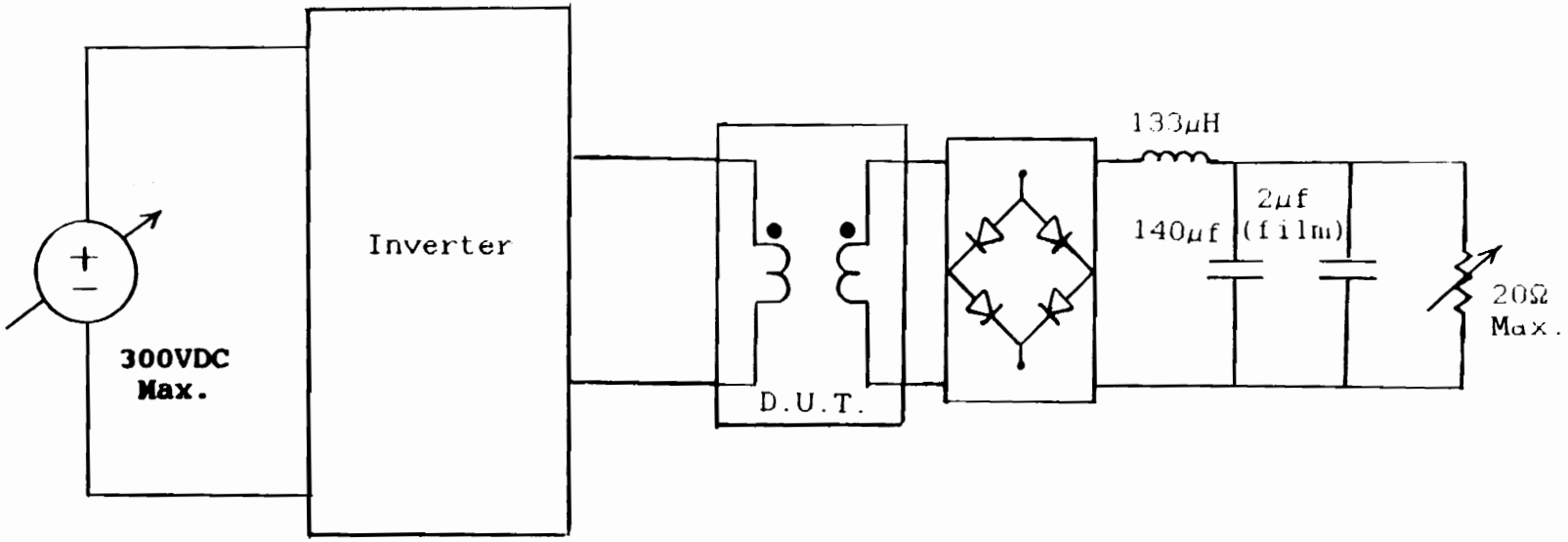

Figure 4.1. Circuit diagram of testing arrangement for transformer.

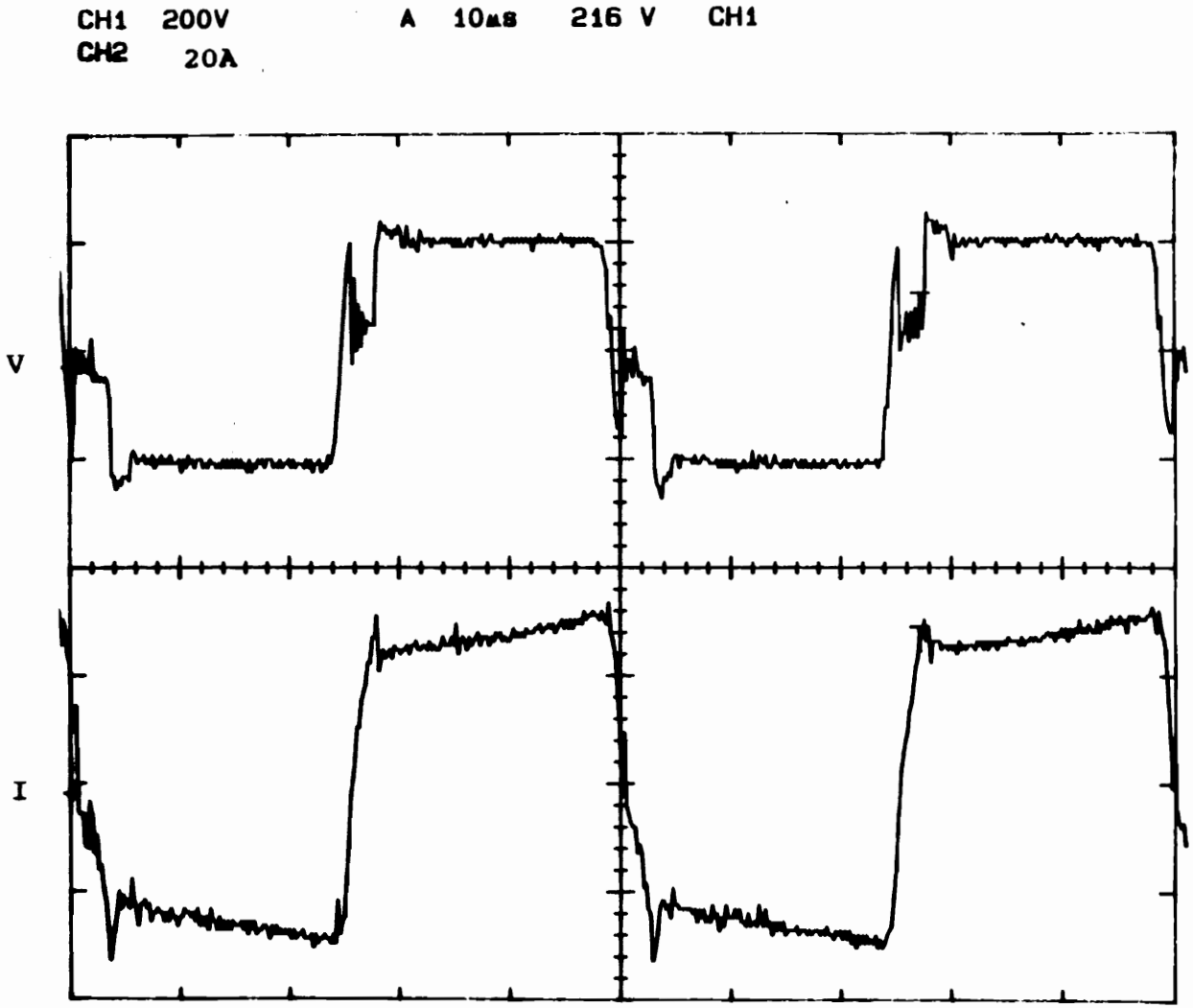

Figure 4.2. Primary voltage and current waveforms

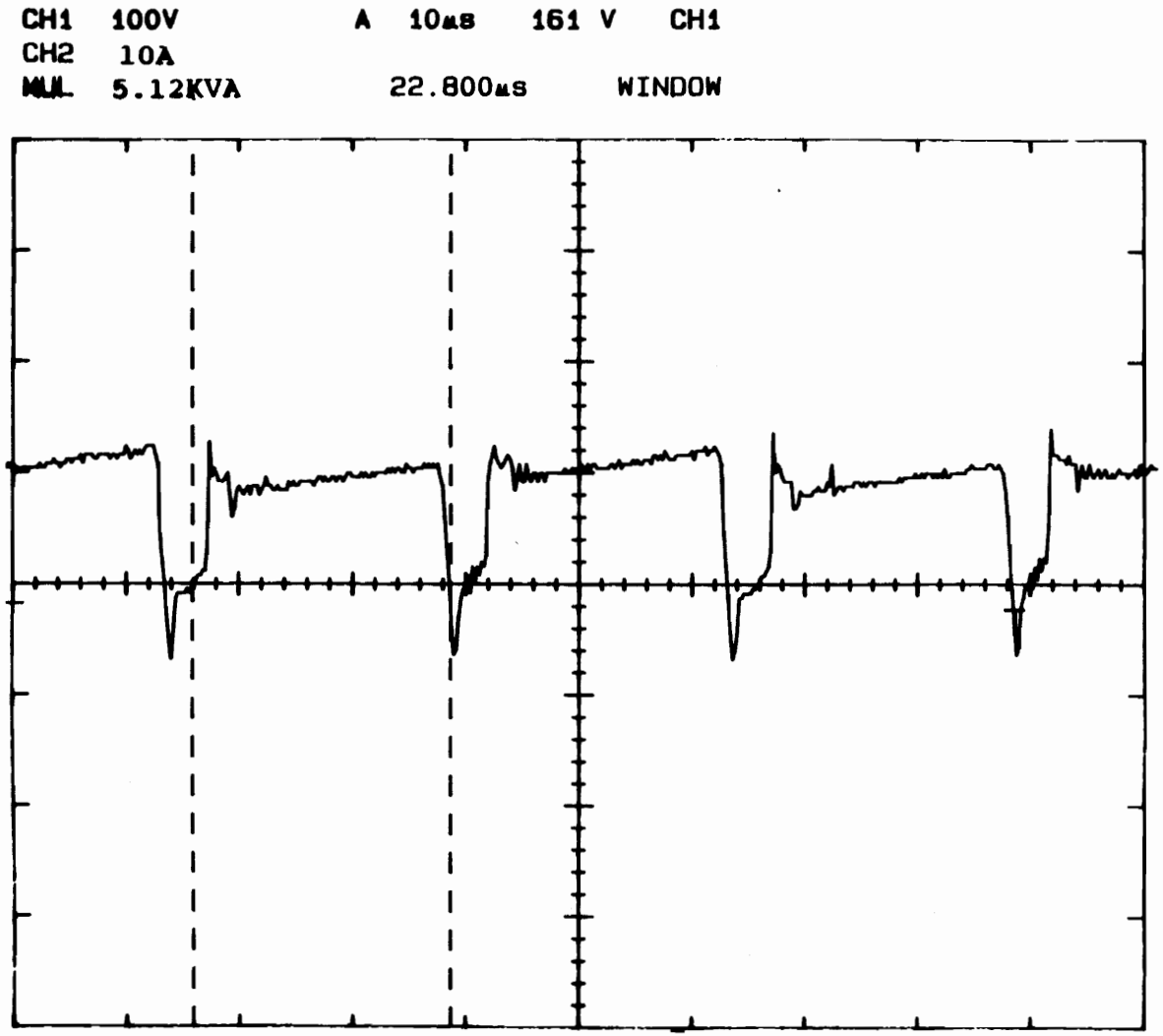

Fig. 4.3. Primary instantaneous power waveform.

yielding the real input power P_{in}. The actual operating frequency of the inverter was measured to be 20.08 kHz. Results of the analysis of Figs. 4.2 and 4.3 are:

V_{pri} = 194.92 volts (rms)

I_{pri} = 26.243 amperes (rms)

energy per cycle = 0.2458 watt-seconds or joules

P_{in} = 0.2458 joules * $20.080*10^3$ Hz = 4935.7 watts

Operating waveforms obtained from the secondary winding are shown in Figs. 4.4 and 4.5. The analysis for these waveforms is the same as for the primary data. The results are:

V_{sec} = 191.44 volts (rms)

I_{sec} = 25.275 amperes (rms)

energy per cycle = 0.2401 watt-seconds or joules

P_{out} = 0.2401 joules * $20.080*10^3$ Hz = 4821.2 watts

Based upon this graphical data, the overall performance is:

$P_{loss} = P_{cu} + P_{core}$ = 4935.7 - 4821.2 = 114.5 watts

efficiency = 4821.2/4935.7 = 97.7%

Fig. 4.6 is a detail of the primary voltage and current. As can be seen, the driving voltage waveform collapses for approximately $2.5*10^{-6}$ seconds after the polarity is switched. This makes the true rise-time of the current difficult to measure. However, the time-delay between the voltage and current when crossing zero is $0.8*10^{-6}$ seconds, and judging by the slope of the current at the crossover point, a rise-time of approximately $1*10^{-6}$ seconds or less seems reasonable.

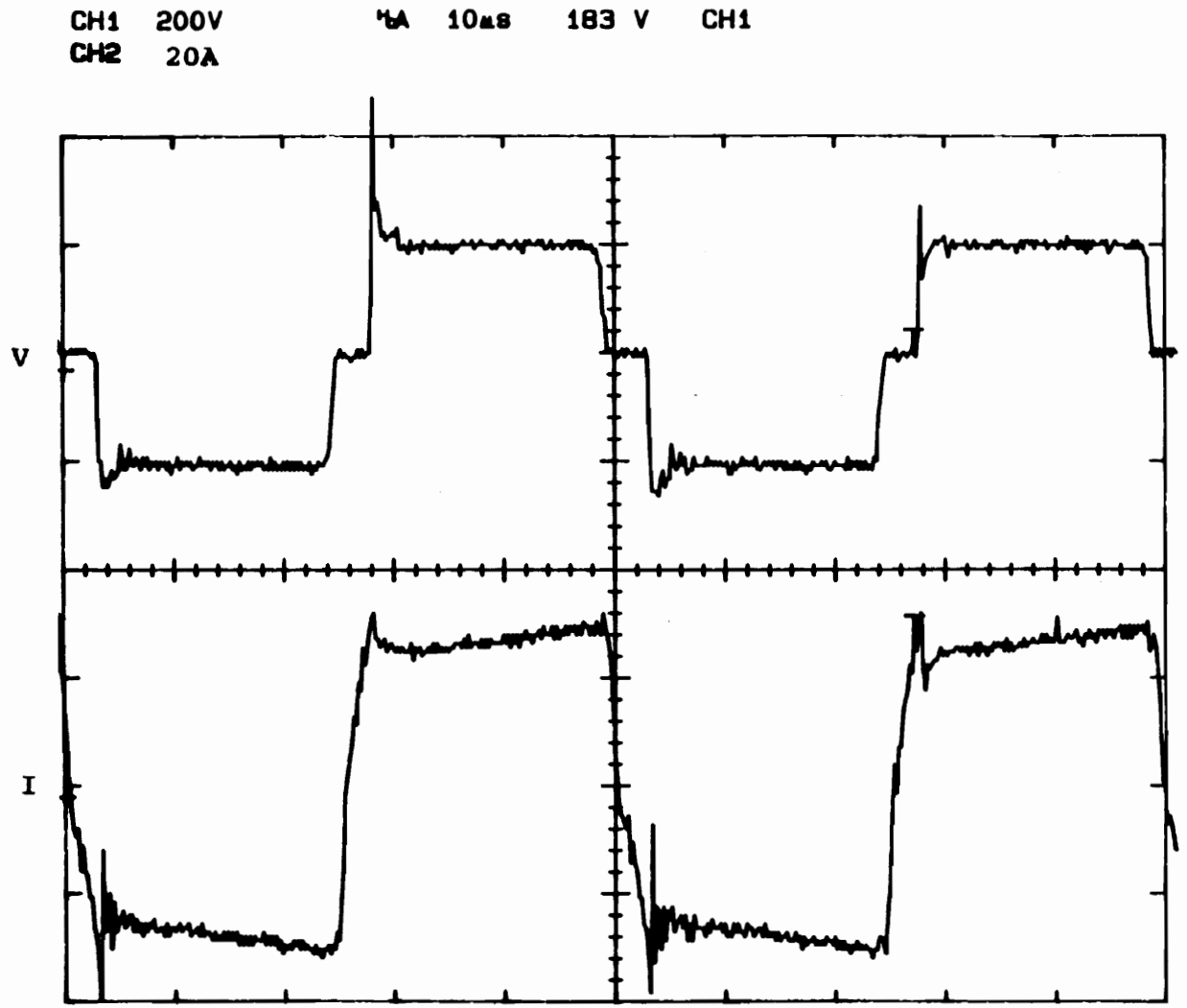

Figure 4.4. Secondary voltage and current waveforms.

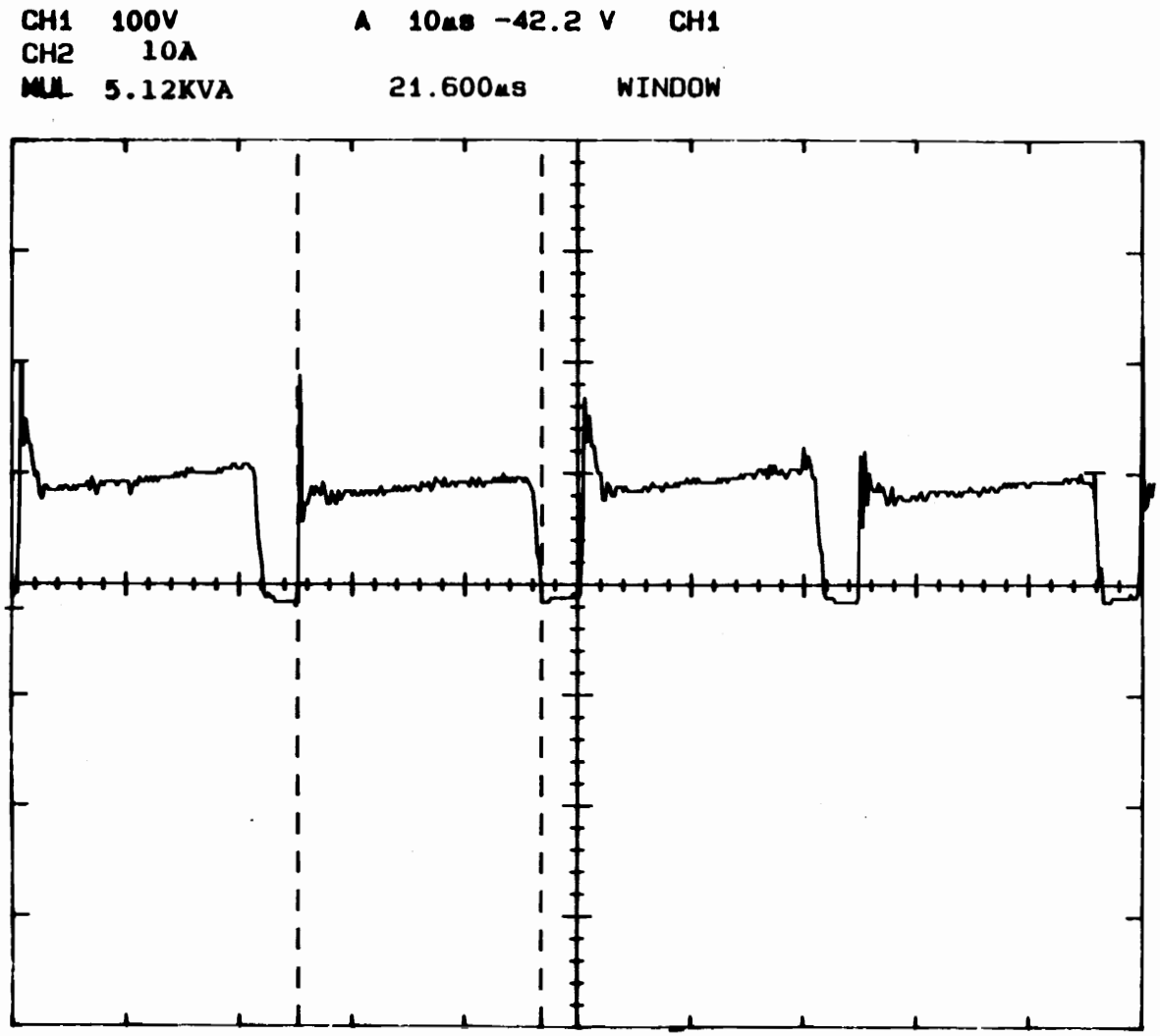

Figure 4.5. Secondary instantaneous power waveform.

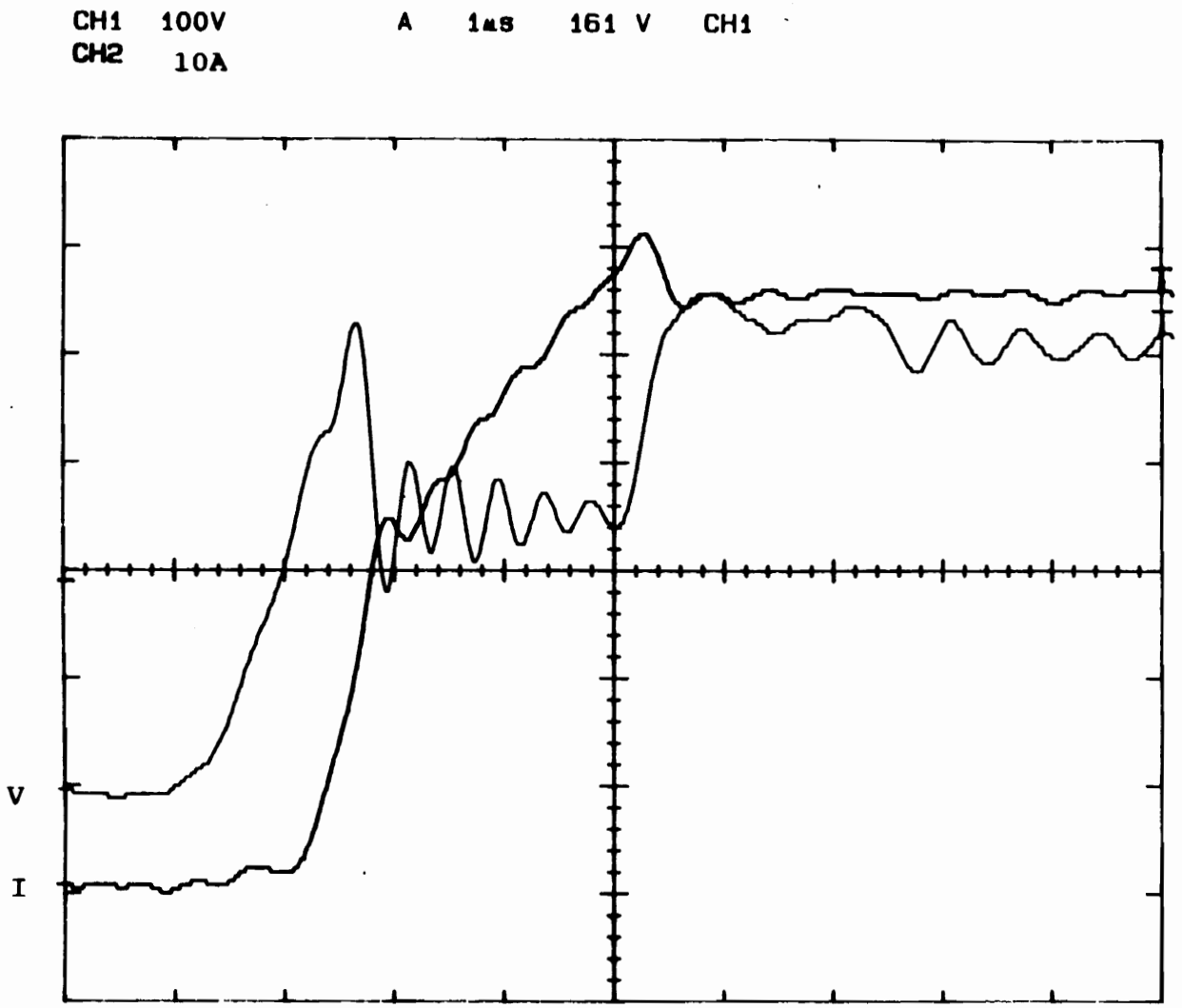

Figure 4.6. Detail of primary voltage and current waveforms for the purpose of observing current rise-time.

4.2 Simulated Operation

To determine the accuracy of the fundamental equivalent circuit shown in Fig. 3.15b, the input voltage and current will be reduced to their fourier equivalents, applied individually to the input of the fundamental model, and the resulting outputs added together. These simulated secondary waveforms will then be compared with the actual waveforms.

Table 4.1 contains the first 12 fourier coefficients and their respective phasor representations for both the current and voltage waveforms of Fig. 4.2. Table 4.2 contains the same harmonic analysis applied to the secondary voltage and current. An AC gain and phase analysis of the fundamental model with a purely resistive load of 8.516 ohms was performed using PSPICE. This load was determined from the fundamental components of the measured secondary voltage and current. The results of this AC analysis are presented in Figs. 4.7a, 4.7b, 4.8a and 4.8b.

Each of the first twelve harmonic components of both the primary voltage and current were modified as dictated by the AC analysis. The simulated secondary waveforms were then reconstructed using the modified input harmonics. The resulting simulated secondary voltage is compared with the actual measured secondary voltage in Fig. 4.9. It should be noted that the comparisons between the simulated an measured

Table 4.1. Fourier coefficients 1 through 12 and the equivalent phasor representations for the primary voltage and current waveforms.

PRIMARY VOLTAGE

HARMONIC	COS TERMS	SIN TERMS	MAGNITUDE	ANGLE (RAD.)	ANGLE (DEG.)
1	-8.76614	262.7556	262.9018	-1.60415	-91.9108
2	8.642933	0.817779	8.681535	-0.09434	-5.40513
3	-7.26434	70.5536	70.92659	-1.6734	-95.8786
4	8.317312	0.558804	8.336063	-0.06708	-3.84368
5	0.152131	22.73488	22.73539	-1.5641	-89.6166
6	8.024322	0.45236	8.037062	-0.05631	-3.22656
7	10.24455	1.56521	10.36343	-0.15161	-8.68674
8	8.358298	3.340138	9.000981	-0.38018	-21.7826
9	19.73411	-5.67434	20.53371	0.279987	16.04206
10	3.062403	8.081901	8.642652	-1.20859	-69.2472
11	24.73917	-1.31688	24.77419	0.05318	3.047007
12	-4.04595	8.710719	9.604495	-2.00563	-114.914

PRIMARY CURRENT

HARMONIC	COS TERMS	SIN TERMS	MAGNITUDE	ANGLE (RAD.)	ANGLE (DEG.)
1	-6.57053	32.32251	32.98358	-1.77134	-101.491
2	-1.3614	-0.36675	1.409934	2.878451	164.9231
3	-3.97856	9.799123	10.576	-1.95647	-112.098
4	-1.19999	-0.55324	1.321384	2.709599	155.2486
5	-3.14706	4.641848	5.608094	-2.16659	-124.136
6	-1.09771	-0.89034	1.413393	2.460129	140.955
7	-2.45029	2.250973	3.327285	-2.39857	-137.428
8	-0.57809	-0.83561	1.016085	2.176014	124.6764
9	-1.8582	0.719344	1.992579	-2.77224	-158.838
10	-0.57624	-0.44683	0.729187	2.482023	142.2095
11	-0.91666	-0.05791	0.918491	3.078503	176.3852
12	-0.80174	-0.4615	0.92508	2.619296	150.0746

Table 4.2. Fourier coefficients 1 through 12 and the equivalent phasor representations for the secondary voltage and current waveforms.

SECONDARY VOLTAGE

HARMONIC	COS TERMS	SIN TERMS	MAGNITUDE	ANGLE (RAD.)	ANGLE (DEG.)
1	1.47853	263.1446	263.1488	-1.56518	-89.6781
2	4.814454	-2.48253	5.416817	0.476081	27.27746
3	-0.15661	73.46092	73.46109	-1.57293	-90.1221
4	1.431471	-5.42274	5.608495	1.312708	75.21263
5	-6.87376	24.65033	25.59077	-1.84274	-105.581
6	-2.23529	-8.56275	8.849704	1.826146	104.6304
7	-9.44238	-2.31976	9.723155	2.900689	166.1972
8	-1.70445	-11.2041	11.33301	1.721766	98.64994
9	-7.49181	-20.2825	21.6219	1.924625	110.2729
10	-0.80167	-10.6902	10.72018	1.645648	94.28868
11	0.644872	-27.9677	27.97515	1.547743	88.67912
12	2.078697	-4.21904	4.703325	1.11301	63.77078

SECONDARY CURRENT

HARMONIC	COS TERMS	SIN TERMS	MAGNITUDE	ANGLE (RAD.)	ANGLE (DEG.)
1	-1.1971	30.8774	30.9006	-1.60955	-92.2202
2	0.323705	-0.10022	0.338863	0.30023	17.20192
3	1.033953	9.671584	9.726695	-1.46429	-83.8979
4	0.01062	-0.35433	0.354494	1.540834	88.28331
5	1.072815	4.709661	4.830304	-1.34683	-77.1675
6	-0.18485	-0.69833	0.722383	1.829562	104.8262
7	0.980915	2.44631	2.635645	-1.18945	-68.1503
8	-0.14764	-1.01989	1.030517	1.714562	98.23716
9	0.919044	1.019968	1.372944	-0.8374	-47.9795
10	-0.16252	-1.08997	1.102022	1.718812	98.48068
11	0.75054	0.111216	0.758736	-0.14711	-8.42881
12	-0.16743	-0.95145	0.966065	1.744989	99.98052

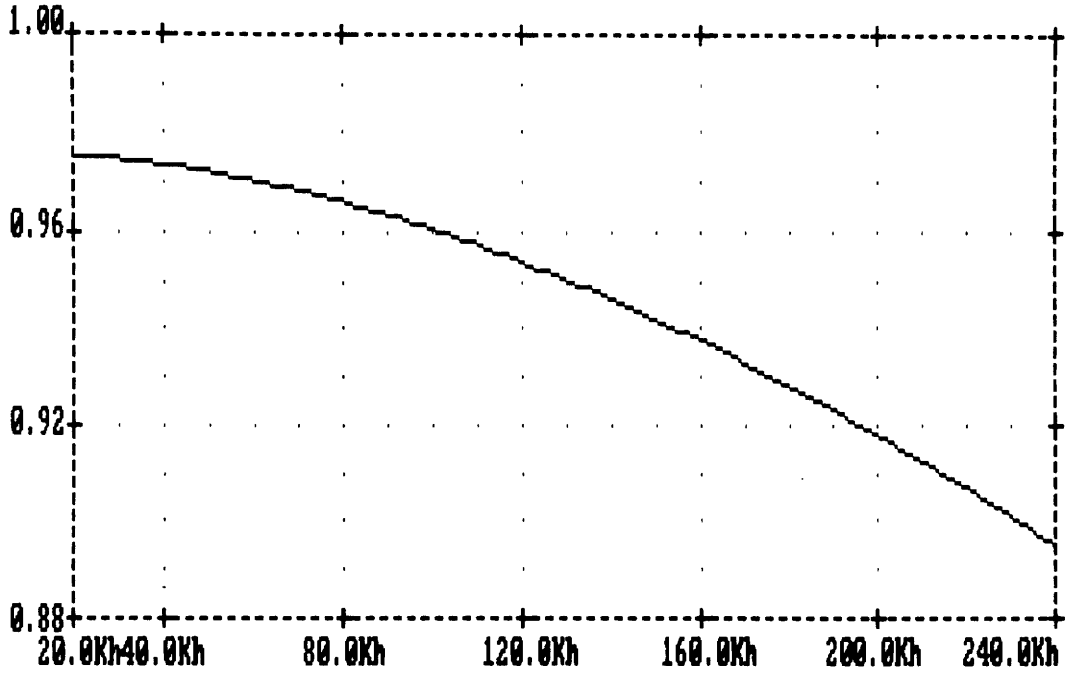

Figure 4.7a. (V_{sec} / V_{pri}) as a function of frequency for the circuit of Fig. 3.15b with a 8.516 ohm load.

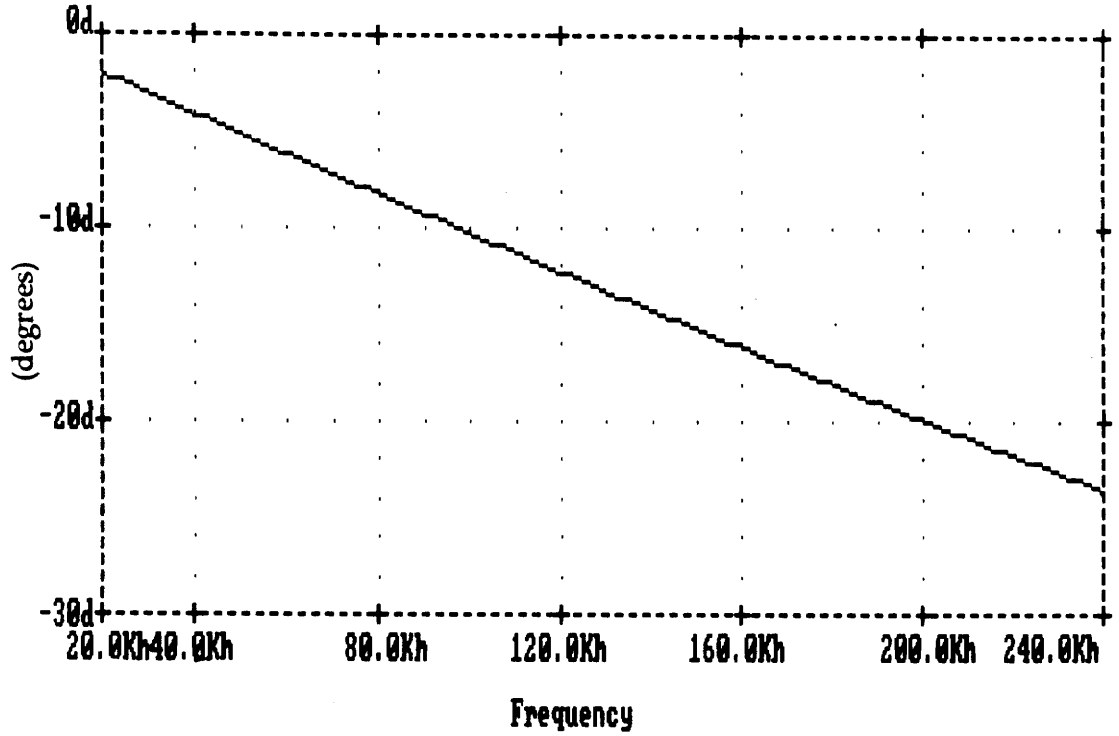

Figure 4.7b. The phase differential in degrees between V_{pri} and V_{sec} for the circuit of Fig. 3.15b with a load of 8.516 ohms.

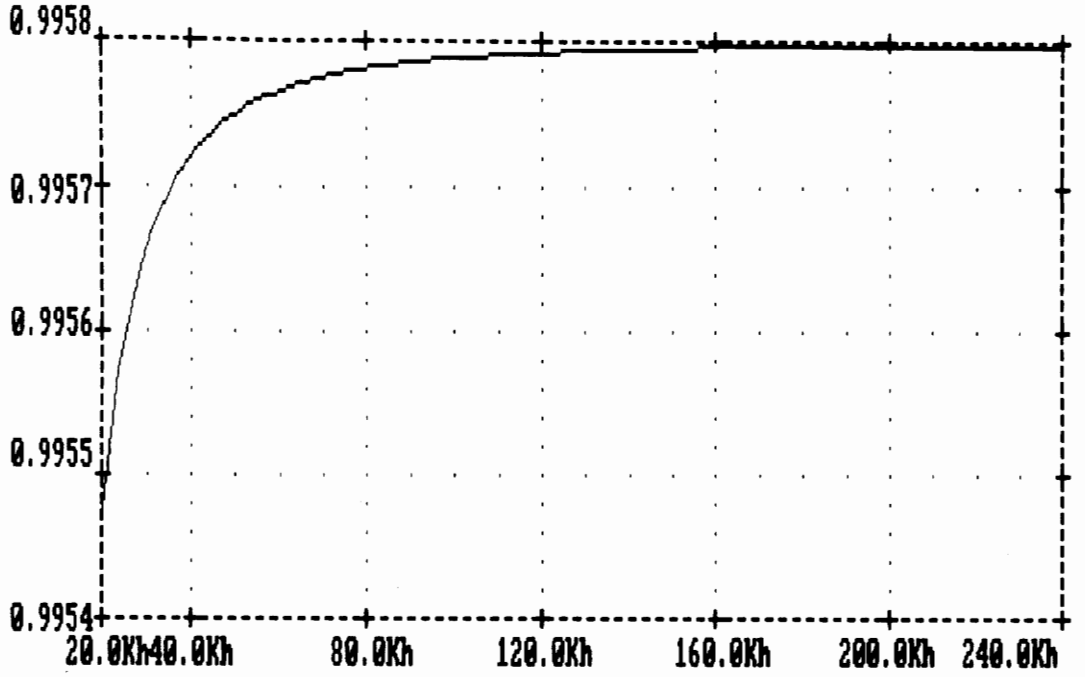

Figure 4.8a. (I_{sec} / I_{pri}) as a function of frequency for the circuit of Fig. 3.15b with a 8.516 ohm load.

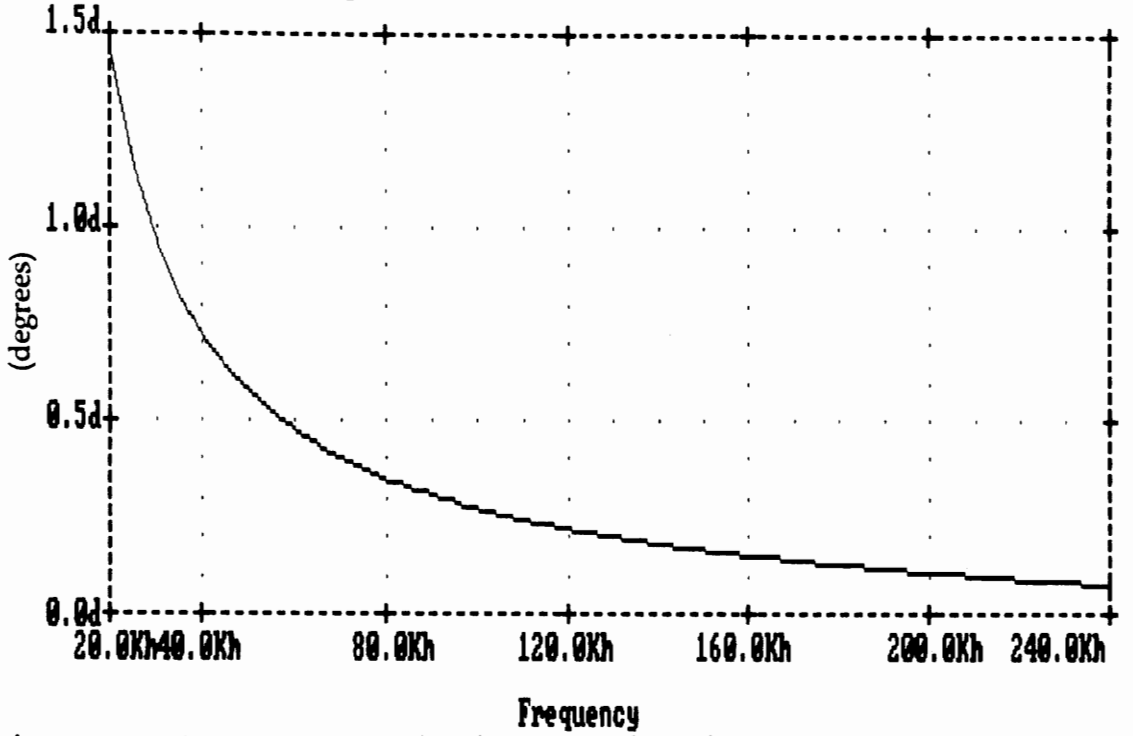

Figure 4.8b. The phase differential in degrees between I_{pri} and I_{sec} for the circuit of Fig. 3.15b with a load of 8.516 ohms.

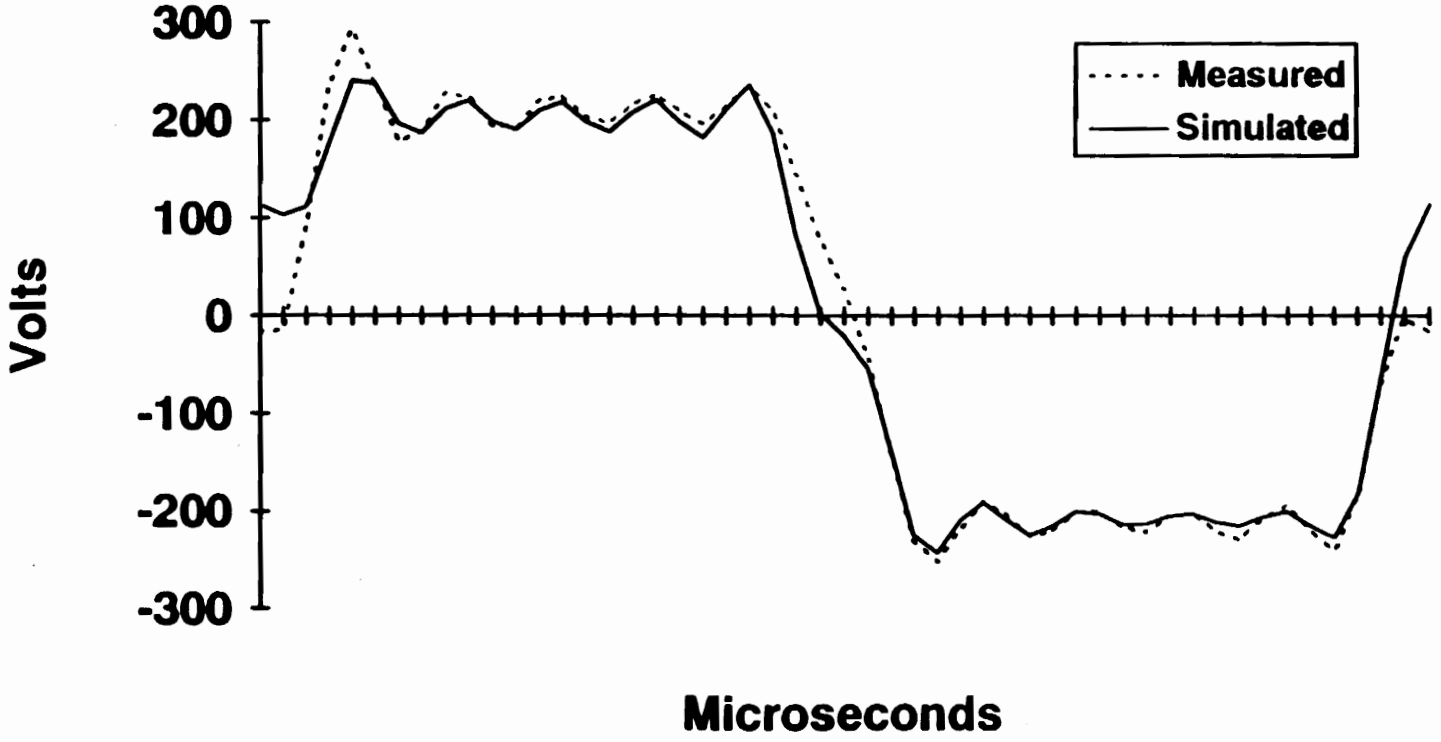

Figure 4.9. Comparison of the simulated and measured secondary voltages.

waveforms are performed using only the first twelve harmonics of each waveform for the purpose of consistency. The comparison between the simulated and measured secondary currents is shown in Fig. 4.10.

For the purpose of simulating the transformer losses, the fundamental model was used in conjunction with the MICRO-CAP circuit analysis program. Each of the first twelve harmonic components of the primary voltage were individually applied to the fundamental model with a 8.516 ohm load. The voltages across each of the resistive elements was calculated with the exception of the load resistance. By determining the voltages, the power lost in each resistance for each harmonic could be determined. All of these losses were then added together to determine the total simulated losses as shown in Table 4.3. This figure excludes any losses attributable to the higher order harmonics, which will be virtually insignificant. The total simulated losses are calculated to be 116.9 watts versus a measured transformer loss of 114.5 watts. This results in a simulation error of:

$$P_{loss} \text{ error} = (116.9-114.5)/114.5 = 2.1\%$$

The transformer was operated at levels as high as 8.25 kVA as shown in Fig. 4.11, but due to limitations of the power supply and the inverter circuit, higher operating power levels could not be attained.

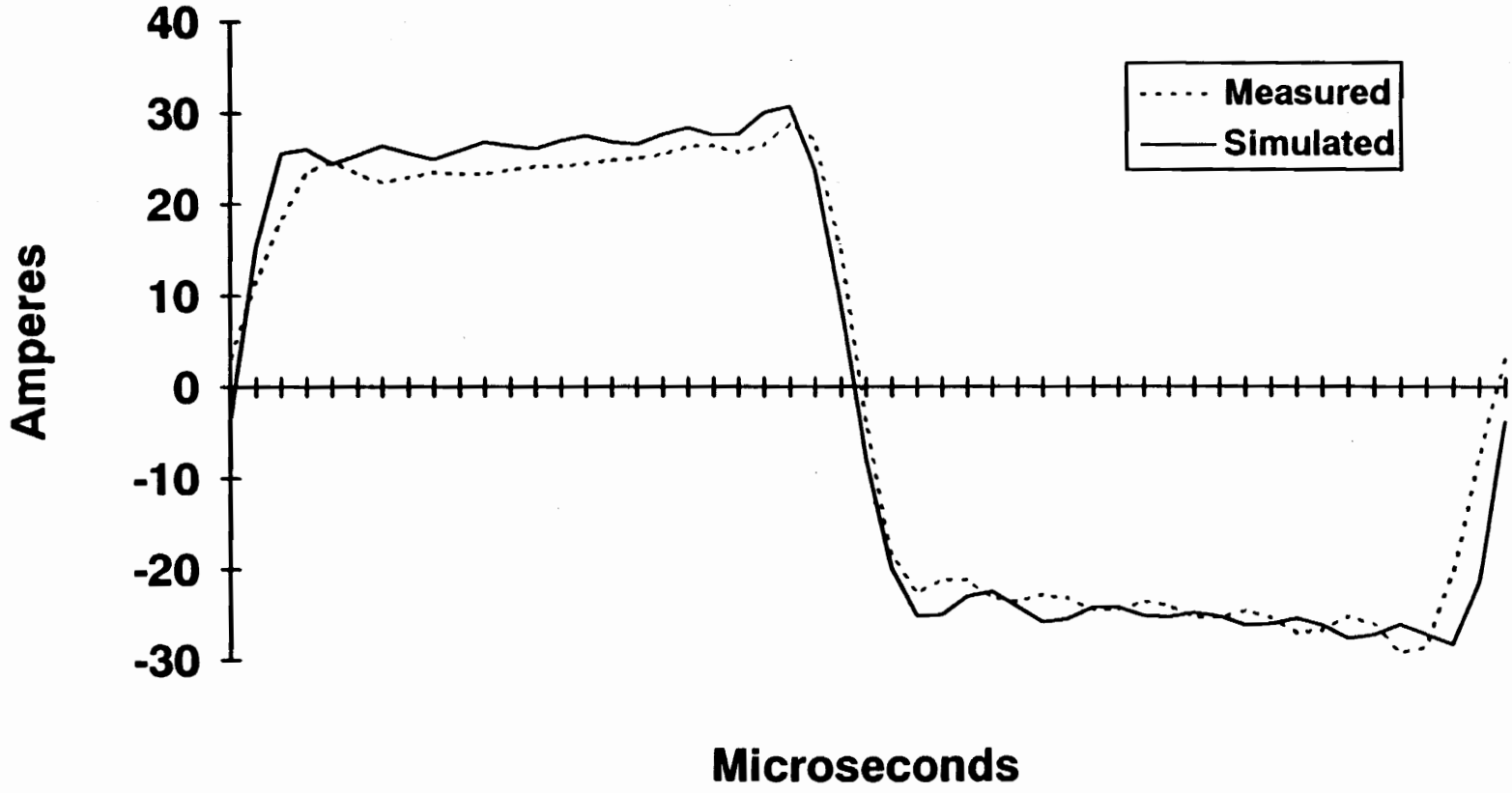

Figure 4.10. Comparison of the simulated and measured secondary currents.

Table 4.3. Simulated transformer losses using the first 12 harmonic components.

HARMONIC	PEAK VRP	PEAK VRS	PEAK VRC	CALCULATED LOSSES
1	3.1	3	260	106.6502
2	0.1	0.1	8.5	0.114529
3	0.8	0.8	65	7.243084
4	0.09	0.09	8	0.09396
5	0.27	0.27	22	0.82563
6	0.09	0.09	8	0.09396
7	0.115	0.115	10	0.152433
8	0.1	0.1	8.7	0.115277
9	0.22	0.22	19.5	0.560969
10	0.095	0.095	8.1	0.103451
11	0.27	0.27	23.5	0.840475
12	0.105	0.105	8.8	0.125787
			TOTAL	116.9198

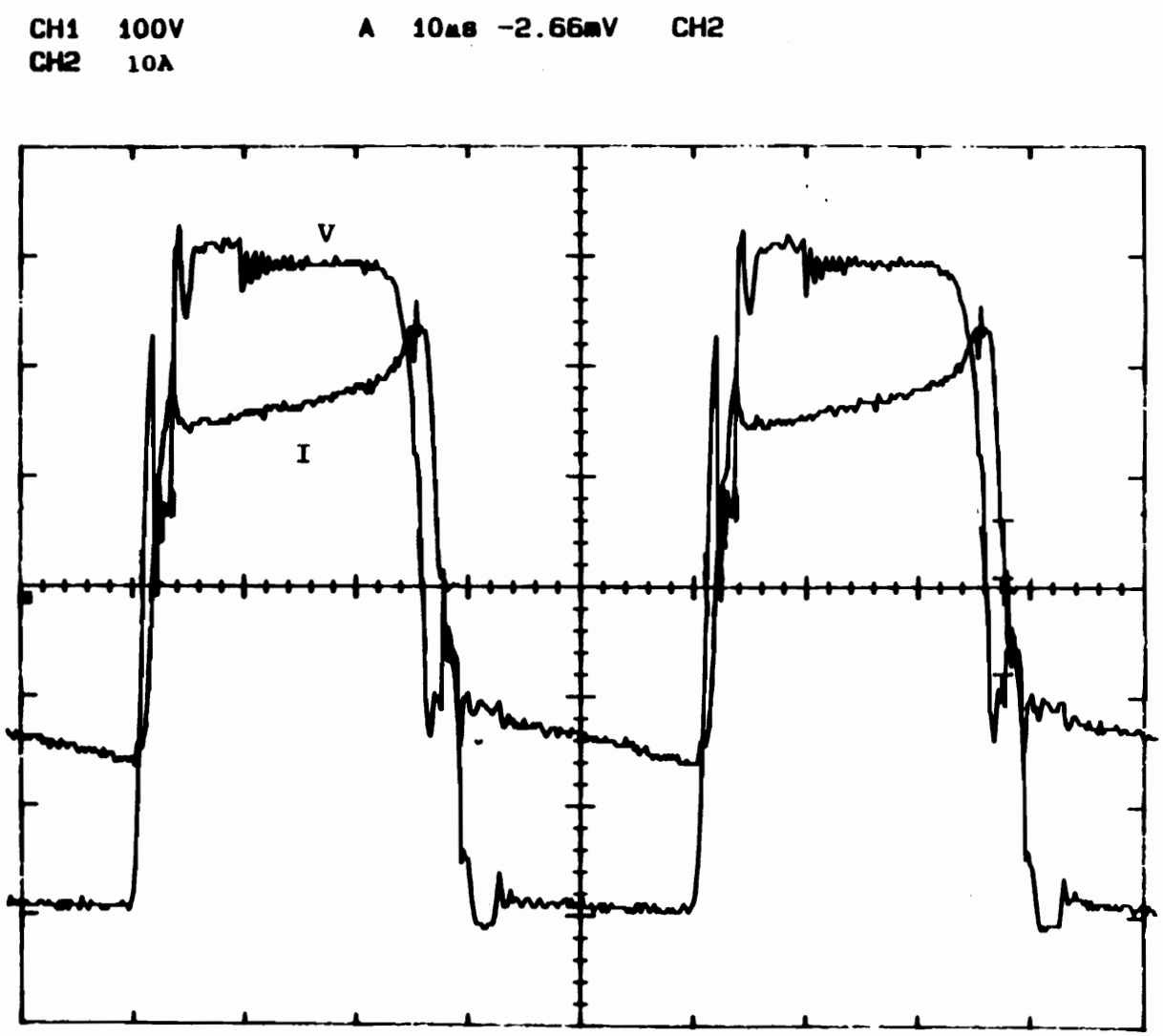

Fig. 4.11. Primary voltage and current waveforms under 8.25 kVA operating conditions.

Chapter 5

The Thermal Model

5.1 Method of Calculating Temperature Rise

There are several ways to determine the temperatures on the surface and within the structure of an electromagnetic device [6,11]. These methods are all based upon the laws of heat transfer and vary with regard to the complexity of the calculations.

If an estimation of the surface temperature is all that is required, the only parameters that need to be known are the transformer surface area and operating loss. By knowing these two parameters, a loss per unit area may be calculated. There are tables available which may then be used to determine the surface temperature rise of a device based upon various ambient temperatures. This method does assume that the core and copper losses may be combined into a total net loss and that the thermal energy is dissipated uniformly over the surface area of the device [6].

It must be noted that the core losses substantially vary with changes in core temperature, and if the fundamental equivalent model is used to determine the operating losses, R_c should reflect the correct core loss at the predicted elevated temperature. The same also holds true for the winding losses, as the resistance of copper increases with

increasing temperature [6].

5.2 Thermal Calculations

Calculation of the surface area of an irregularly wound toriodal transformer requires some degree of approximation. Fig. 5.1 illustrates the cross-section of the transformer being analyzed. The surface area may be calculated by separating the transformer into an equivalent torus and cylinder as shown in Fig. 5.2.

The equation for the surface area of a torus is:

$$S_T = 4\pi^2 Rr \qquad (5.1)$$

and the equation for the inner and outer surface areas of the cylinder is:

$$S_c = 4\pi hR \qquad (5.2)$$

The physical dimensions corresponding to the transformer shown in Fig.5.2 are:

$$R = 3.375*10^{-2} \text{ meters}$$

$$r = 2.875*10^{-2} \text{ meters}$$

$$h = 3.25*10^{-2} \text{ meters}$$

which when substituted into Eqs. 5.1 and 5.2 yield:

$$S_T = 3.83*10\text{-}2 \text{ m}^2$$

$$S_c = 1.38*10\text{-}2 \text{ m}^2$$

The gaps between the turns on the outer radius of the cylinder and the torus must also be considered. At first glance these spacings do not appear significant, however they

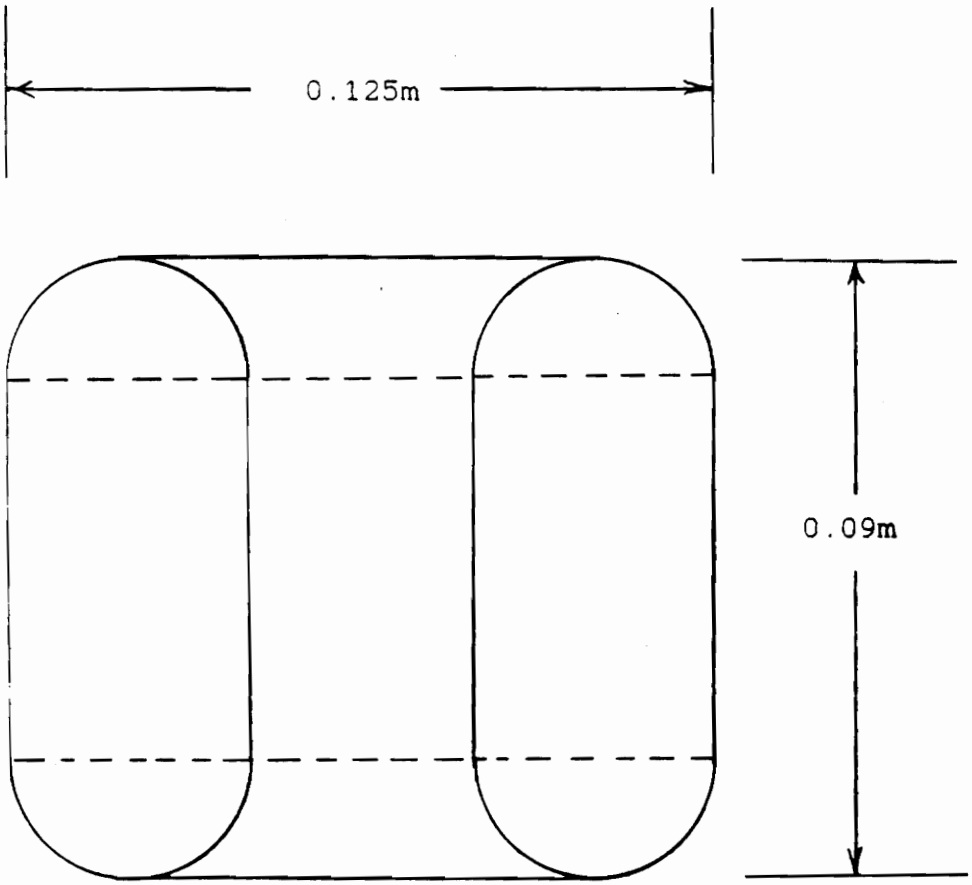

Figure 5.1. Transformer cross-section.

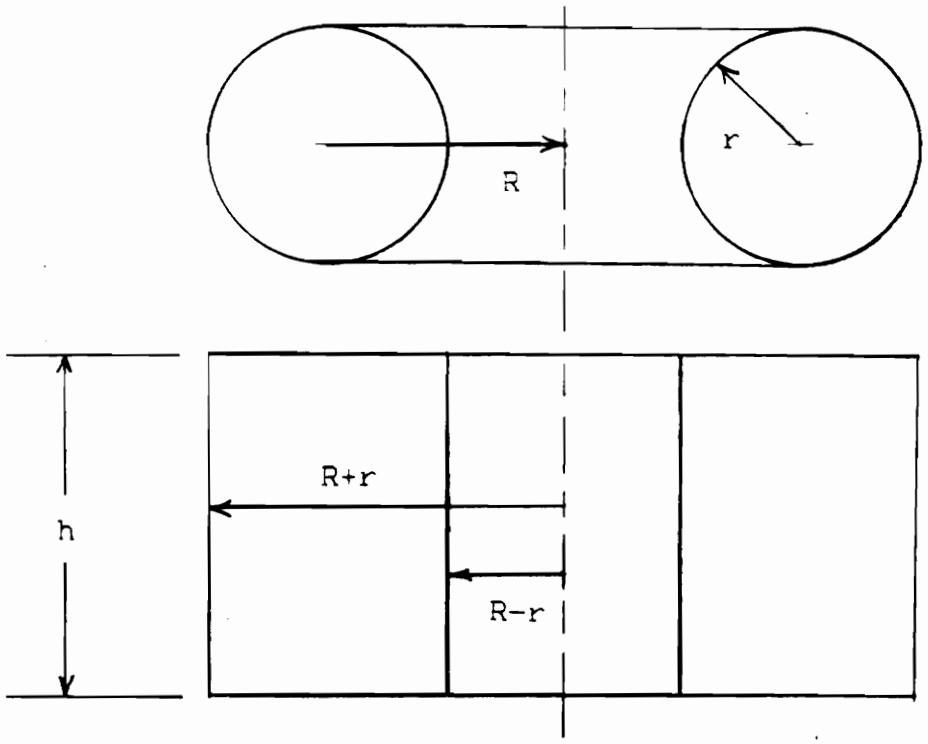

Figure 5.2. Torus and cylinder used in the calculation of the transformer surface area.

serve the same purpose as the fins of a heat sink. Fig. 5.3 illustrates a portion of the cross-section of the transformer. The depths of the gaps between adjacent turns reach to the core surface. Half of the added surface area per gap may be calculated by subtracting the cross-sectional areas of the core and inner portion of the winding between the core and center of the transformer from that of the total transformer. This yields a total added area per gap (S_G) of:

$$S_G = 2(\pi r^2 + 2rh - (T_t + IW_t)T_h) \qquad (5.3)$$

where T_t and T_h are the transformer core thickness and height, and IW_t is the thickness of the inner portion of the winding. These dimensions are:

$$T_t = 1.05*10^{-2} \text{ meters}$$

$$T_h = 7.0*10^{-2} \text{ meters}$$

$$IW_t = 2.0*10^{-2} \text{ meters}$$

which when substituted into Eq. 5.3 result in:

$$S_G = 4.66*10^{-3} \text{ m}^2$$

By inspection of the device it is determined that there are 16 gaps between the turns on the outer radius, therefore the total estimated surface area of the transformer is:

$$S_T + S_C + (16*S_G) = 12.67*10^{-2} \text{ m}^2$$

As previously mentioned, it is necessary to change R_c to a value which is more indicative of the core losses at the estimated elevated core temperature. Section 3.8.5 outlined the method for calculating the core loss by use of the loss curves of Fig. 3.10. The only difference in calculating the

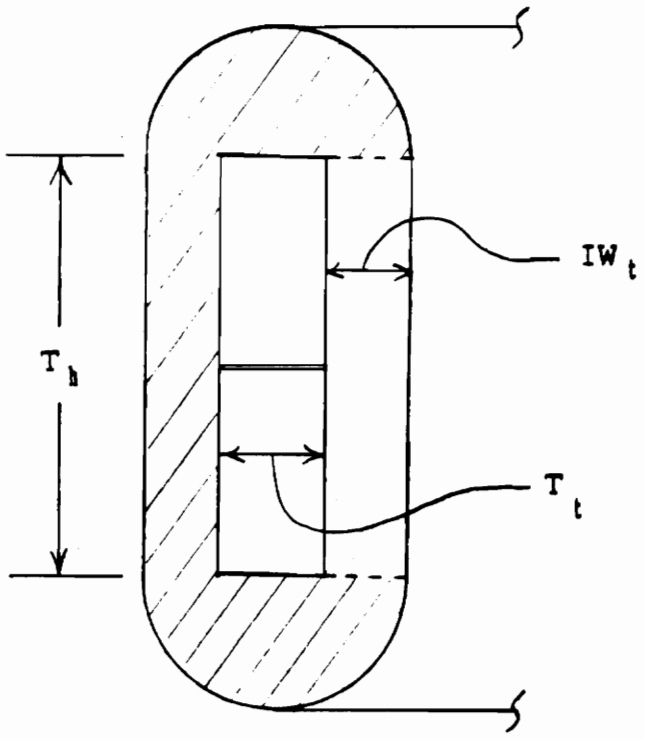

Figure 5.3. Partial cross-section of transformer illustrating additional surface area due to gaps between adjacent turns.

new value of R_c is that the 100°C curves should be used instead of the 23°C data since it is logical to assume that the actual core temperature will be closer to the higher value. The revised core loss P_f is:

$$P_f = 14 \text{ watts/kg} * 0.8 \text{ kg} = 11.2 \text{ watts}$$

This new value of R_c is therefore:

$$R_c = (200 \text{ volts})^2 / 11.2 \text{ watts} = 3571.43 \text{ ohms} \qquad (5.4)$$

The increase in copper temperature must also be considered. As the thermal data will reveal, the outer surface temperature reaches a level of approximately 70°C and the inner or core temperature reaches a level of slightly over 90°C. It is logical to speculate that the copper temperature is somewhere between the two extremes, and for estimation purposes a temperature of 80°C will be assumed. The increase in resistance due to 80°C copper temperature is approximately 25% [6]. As a result, the values of R_p and R_s that should be used for simulation are:

$$R_p = R_s = 1.25*0.1012 = 0.1265 \text{ ohms} \qquad (5.5)$$

The load resistance was increased to limit the temperature rise of the transformer during the thermal testing. It was feared that without the transformer being within a thermally conducting media suited for high dissipation, a thermal runaway condition could occur at the 5kVA level. Adjustments were made so that the transformer operated near the 4kVA level for this test.

Using the fundamental model of Fig. 3.15b supplied with

the new values of R_c, R_p and R_s found in Eqs. 5.4 and 5.5, it was calculated that the total losses with the increased load were 76.41 watts. This gives a surface power density (SPD) of:

$$SPD = 76.41 \text{ watts} / 12.67*10^{-2} \text{ m}^2 = 603.1 \text{ watts/m}^2$$

Using the temperature rise versus surface dissipation data presented in Fig. 5.4, it was determined that the rise was approximately 45.3°C. A 26.6°C ambient temperature was measured prior to the beginning of the thermal test giving a predicted surface temperature (PST) of:

$$PST = 45.3^\circ C + 26.6^\circ C = 71.9^\circ C$$

Thermocouples were placed in the locations indicated in Fig. 5.5 to monitor the outer surface temperature and the core temperature. The core temperature was measured to ensure that it did not rise to a level which would allow saturation. Both sets of data are plotted versus time in Fig. 5.6 along with the predicted surface temperature level calculated above. The error between the steady-state calculated and measured values is therefore:

$$\% \text{ error} = (71.9^\circ C - 70^\circ C) / 70^\circ C = 2.7\%$$

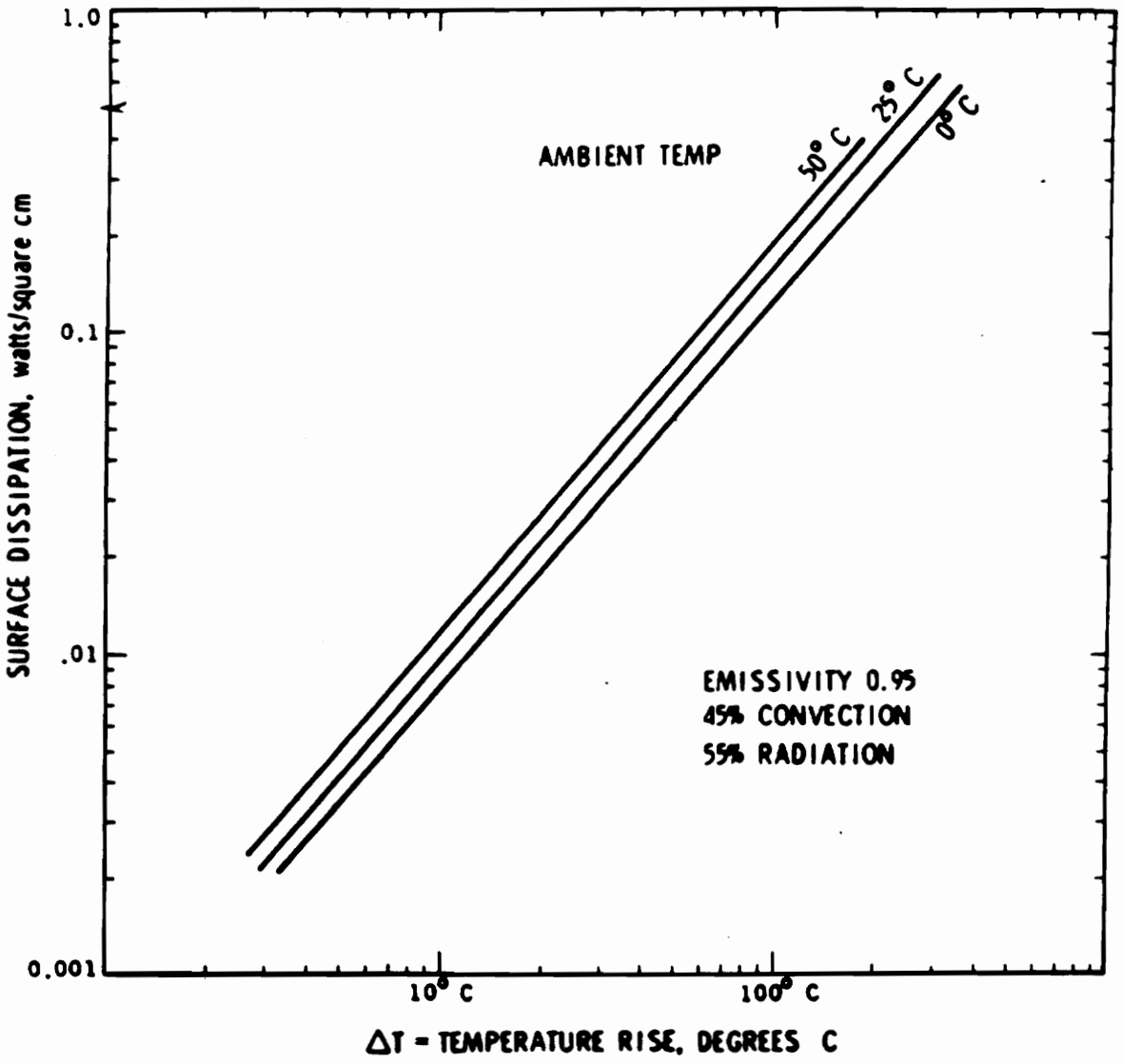

Figure 5.4. Temperature rise vs. surface dissipation [6].

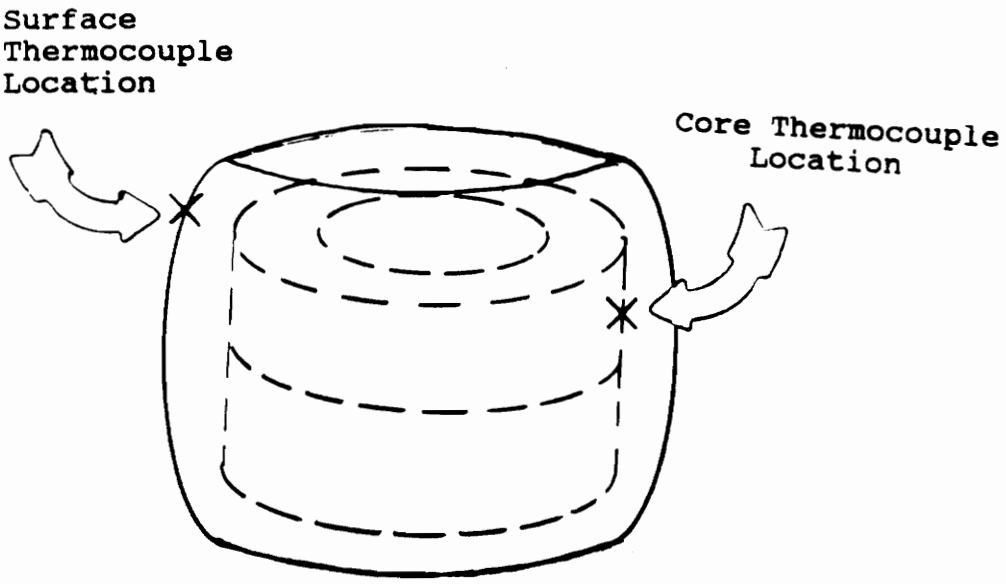

Figure 5.5. Thermocouple locations used during thermal test.

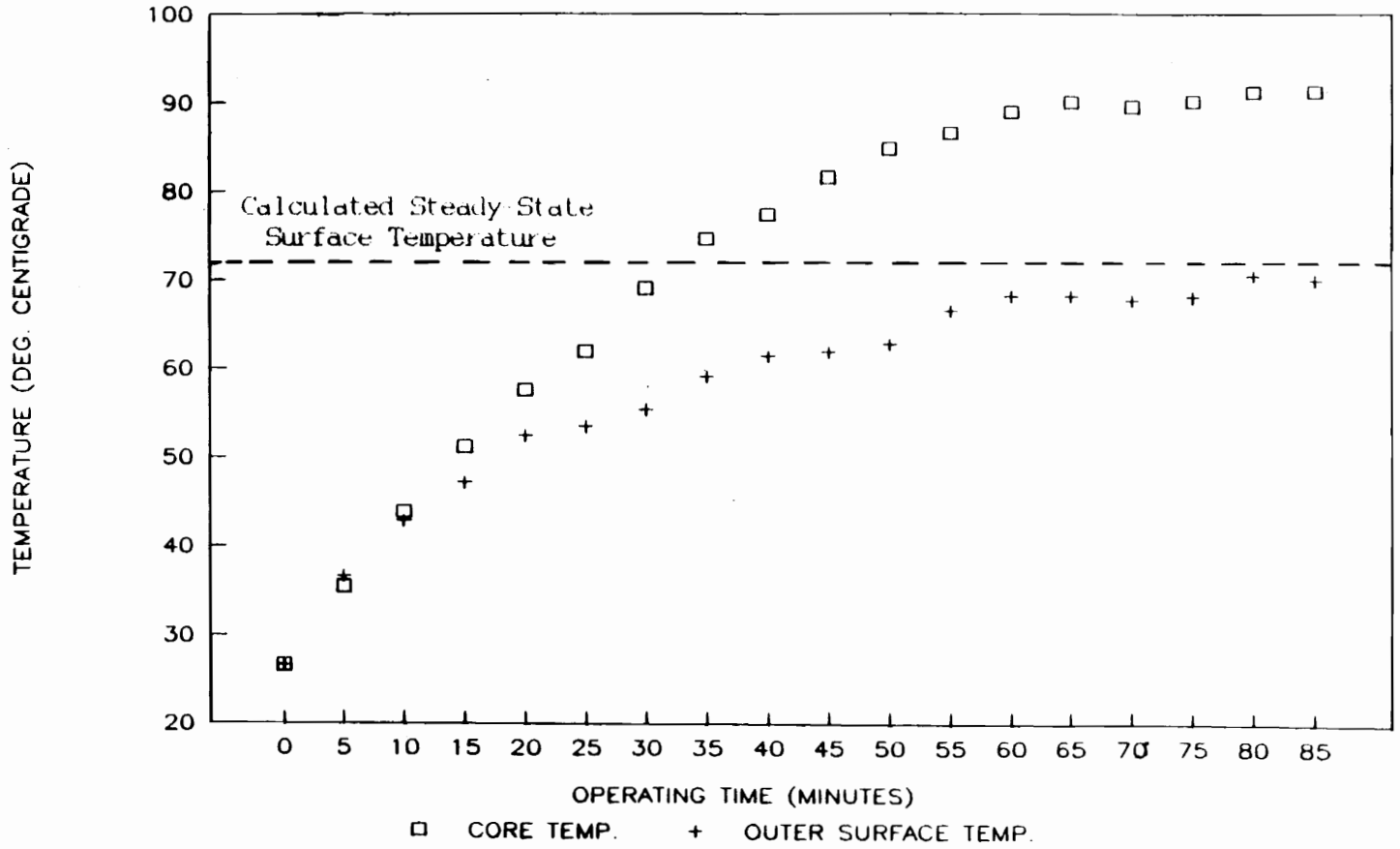

Figure 5.6. Measured transformer surface and core temperatures vs. time, and calculated steady-state surface temperature.

Conclusions

Transformer design has both fixed and variable aspects. Faraday's and Ampere's Laws are absolutes and are the cornerstone of electromagnetic design, however the choice of materials and winding techniques have a tremendous impact upon the robustness of a design, especially at high-frequencies. The method of construction directly impacts winding losses, leakage inductance, distributed capacitances and interwinding capacitance which all have varying effects upon performance.

In this paper, the electromagnetic equations for transformer design were developed from the basic laws and a systematic procedure was outlined for designing a toroidal power transformer. Also, the skin and proximity effects encountered in windings were reviewed and used as a basis for the estimation of the current redistribution within a conductor.

The high-frequency equivalent transformer circuit was developed as well as the methods for predicting the various equivalent circuit elements. Two of the circuit parameters, core loss resistance and magnetizing inductance, were calculated using formulas which apply to all transformers regardless of winding configuration. The other parameters are all very dependent upon the winding structure and were determined from equations developed for this particular design. By experimentation, the actual equivalent circuit

elements were determined using the fundamental components of the driving and resulting waveforms. The calculated and measured values of the equivalent circuit elements were then compared to determine the accuracy of the calculations. Errors ranged from 0.3% for the interwinding capacitance, to 30.6% for the leakage inductance.

Simulations were performed using the fundamental model for the purpose of determining the winding and core losses. These losses were compared to the measured losses revealing an error of 2.1%. As a further test of the model, the actual input voltage and current waveforms were applied to the fundamental equivalent circuit and the output waveforms were compared to the actual recorded waveforms with moderate success.

The fundamental model was used to determine the losses at a different operating level for the purpose of solving the temperature rise problem. A method for determining the steady-state surface temperature of a body was employed which is based upon total losses and the approximate surface area of the body. The results of this calculation yielded a surface temperature of just 2.7% above the measured quantity.

This research provided an overall view of high-frequency power transformer design and analysis as well as offered an alternative winding method for the reduction of winding losses and leakage inductance. Materials have been developed which help alleviate the loss and leakage problems including Litz wire and foil conductors, unfortunately these aids are

relatively expensive and in many cases are physically not suitable for the core structures being used.

The transformer was never tested at the 10 kVA level due to circuitry and power supply limitations. However, there were limited measurements taken at a 8.25 kVA level, giving proof that the transformer design was functional in free air for a limited period of time at that point. For this transformer to operate on a continuous basis at this level or greater, it would be necessary to place it in a thermally conductive environment which would compensate for the higher losses.

It is suggested that areas of further research might include:

* alternative winding methods to reduce winding losses
* effects of conductor temperature upon current density distribution
* different core structures used at high-power levels
* and the increase of power levels of a device encased or immersed in various thermally conducting media.

Appendix A

Nomenclature Used in this Thesis

Table A.1. Description of symbols used in this thesis.

Symbol	Description
δ	skin depth
$\delta\Phi$	change in flux
δT	period of time corresponding to $\delta\Phi$
ϵ_0	permittivity of free space
λ	flux linkage
μ	permeability
μ_0	permeability of free space
μ_i	initial permeability
Φ	flux
A	cross-sectional area
A_c	transformer core cross-sectional area
A_{DC}	cross-sectional area of copper within a single wire
A_E	elliptical area

Table A.1. Description of symbols used in this thesis, continued.

A_c	cross-sectional area of single core
A_{se}	effective conduction area of a single wire due to skin effect
B	flux density
B_s	saturation flux density
C	capacitance
C_{12}	interwinding capacitance
CD	copper diameter
CF	winding correction factor
C_p	primary distributed capacitance
C_s	secondary distributed capacitance
d	effective diameter of braided conductor
D	distance between centers of conductors
D.U.T.	device under test
f	frequency
F_{xps}	external proximity effect factor

Table A.1. Description of symbols used in this thesis, continued.

F_{IPE}	internal proximity effect factor
F_{SE}	skin effect factor
h	cylinder dimension
H	magnetic intensity
H_1	magnetic field generated by I_1
H_e	externally applied magnetic field
Ht	height of single core
I	current
I_1	conductor current
ID	inner diameter of core
I_e	eddy currents giving rise to skin effect
I_{fund}	fundamental current component
I_p	eddy currents giving rise to proximity effect
I_{pri}	primary current
I_{sec}	secondary current

Table A.1. Description of symbols used in this thesis, continued.

IW_c	inner winding thickness
l	length
L	inductance
L′	length of twisted winding
L_ϕ	magnetizing inductance
l_1	vertical dimension of primary/secondary bundle
l_2	horizontal dimension of primary/secondary bundle
l_c	transformer core length
l_e	effective core length
L_p	primary leakage inductance
L_s	secondary leakage inductance
L_T	total leakage inductance
MLT	mean-length turn
MMF	magnetomotive force
N	number of turns
OD	outer diameter of core

Table A.1. Description of symbols used in this thesis, continued.

ρ	density
P_{core}	core losses
P_{cu}	winding losses
P_f	calculated core losses from manufacturer's data
P_{in}	input power
P_{loss}	transformer losses
P_{out}	output power
PST	predicted surface temperature
r	torus dimension
R	torus dimension
R'	reluctance
RAD_{eff}	effective radius of braided conductor
R_c	core loss resistance
R_{DC}	D.C. winding resistance
R_{HF}	equivalent high-frequency resistance

Table A.1. Description of symbols used in this thesis, continued.

R_p	primary winding resistance
R_s	secondary winding resistance
R_T	total winding resistance
S_c	inner and outer cylinder surface areas
S_G	additional surface area due to one gap
SPD	surface power density
S_T	torus surface area
t	time
T_c	curie temperature
T_h	total core height
T_t	core thickness
μ	permeability
μ_o	permeability of free space
V	voltage
v	volume
V_{fund}	fundamental voltage component

Table A.1. Description of symbols used in this thesis, continued.

V_p	primary voltage (rms)
V_{pri}	primary voltage
VRC	core loss resistance voltage
V_{rms}	root-mean-square voltage
VRP	primary resistance voltage
VRS	secondary resistance voltage
V_{sec}	secondary voltage
w	radian frequency
W	energy
W_2	energy stored in 2 turns
WD	wire diameter
W_T	total winding energy
Z_{rms}	fundamental impedance

Appendix B

Data for Conversion of English to RMKS System of Units

Table B.1. Conversion Data

To Convert From	To	Multiply By
Inches	Meters	$2.54*10^{-2}$
Sq. Inches	Sq. Meters	$6.452*10^{-4}$
Cir. Mils	Sq. Meters	$5.067*10^{-10}$
Cub. Inches	Cub. Meters	$1.639*10^{-5}$
Pounds	Kilograms	0.4535
Lines	Webers	$1*10^{-8}$
$\frac{\text{Lines}}{\text{Sq. Inch}}$	Tesla	$1.55*10^{-5}$
$\frac{\text{Ampere-Turn}}{\text{Inch}}$	$\frac{\text{Ampere-Turn}}{\text{Meter}}$	39.37

Appendix C

Additional Ferrite Data

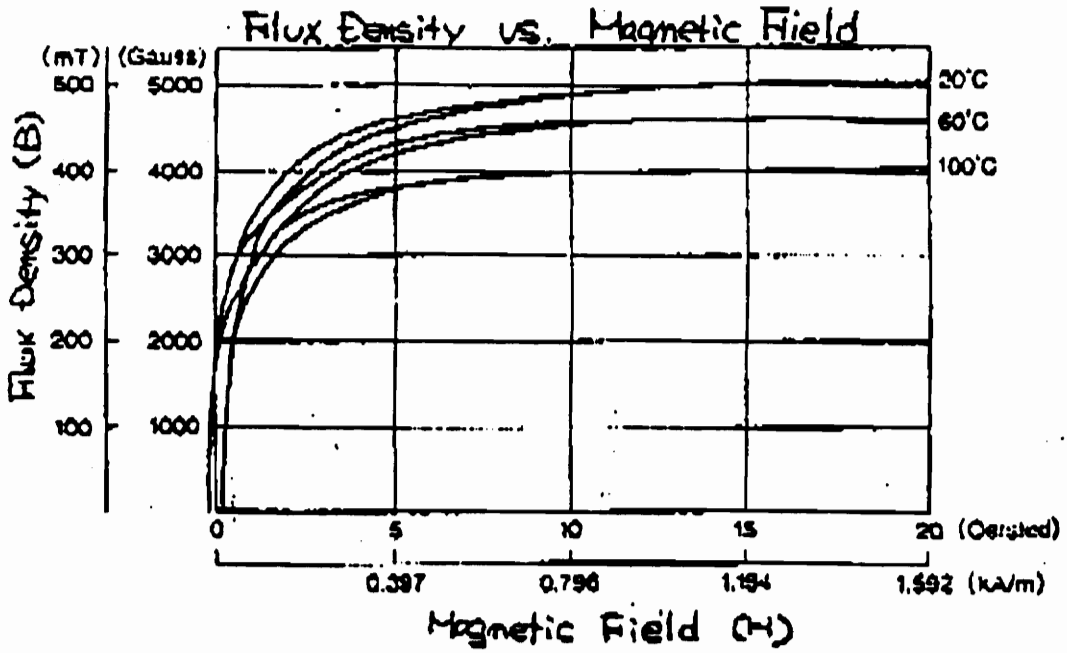

Figure C.1a. Magnetization curves (TDK PE-1).

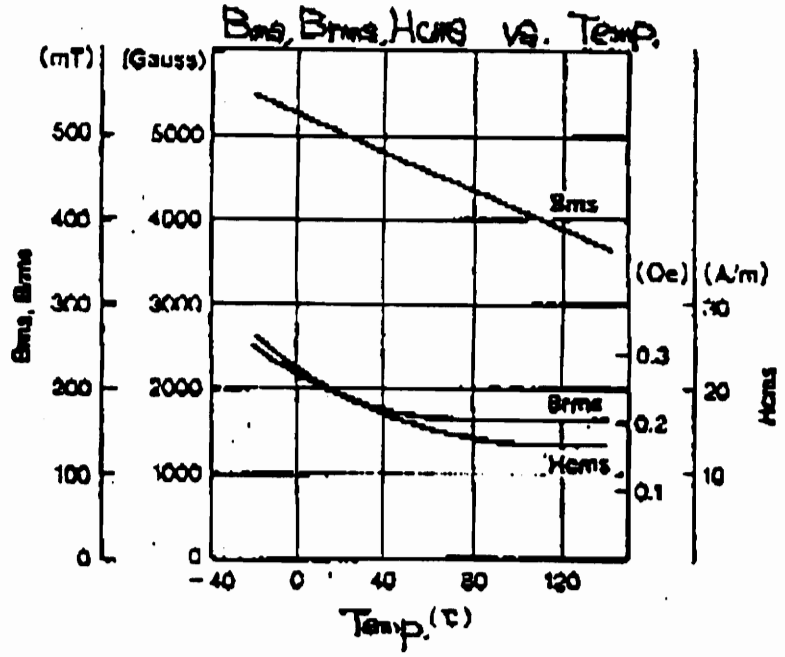

Figure C.1b. Bms (B_s) vs. temperature (TDK PE-1).

REFERENCES

[1] John D. Krauss, Electromagnetics, New York: McGraw-Hill Book Company Inc., 1953, Chapters 3,4, and 5.

[2] Gordon R. Slemon, Magnetoelectric Devices: Transducers, Transformers, and Machines, New York: John Wiley and Sons, Inc., 1966, Chapters 1,2, and 3.

[3] George McPherson, An Introduction to Electrical Machines and Transformers, New York: John Wiley and Sons, 1981, Chapter 3.

[4] Reference Data for Radio Engineers, Editor: H.P. Westman, Indianapolis: Howard W. Sams and Company Inc., 1970, pp. 6.4-6.8, 42.1-42.14.

[5] E.A. Loew, Direct and Alternating Currents, New York: McGraw-Hill Book Company Inc., 1954, Chapter 25.

[6] William T. McLyman, Transformer and Inductor Design Handbook, New York: Marcel Dekker Inc., 1988, pp. 261-270, 277-288.

[7] A.W. Lofti, P.M. Gradzki, and F.C. Lee, "Proximity Effects in Coils for High Frequency Power Applications",

Proceedings of The Tenth Annual VPEC Power Electronics Seminar, pp. 29-31 (1992).

[8] Magnetic Properties of Materials, Editor: Jan Smit, New York: McGraw-Hill Book Company Inc., 1971, pp. 90-97.

[9] H.M. Schlicke, Essentials of Dielectromagnetic Engineering, New York: John Wiley and Sons, Inc., 1961, pp. 2-5, 46-47.

[10] George M. Attura, Magnetic Amplifier Engineering, New York: McGraw-Hill Book Company, Inc., 1959, pp. 49-65, 67-73.

[11] E.C. Snelling, Soft Ferrites: Properties and Applications, London: Butterworth and Company, 2nd Ed., 1988, Chapters 2,4,9 and 11.

[12] Audrey M. Urling, Van A. Niemela, Glenn R. Skutt, Thomas G. Wilson, "Characterizing High-Frequency Effects in Transformer Windings - A Guide to Several Significant Articles." IEEE APEC Proceedings, pp. 373-385 (1989).

[13] Marty Brown, Practical Switching Power Supply Design, San Diego: Academic Press Inc., 1990, pp. 67-83, 189-198.

[14] John G. Kassakian, Martin F. Schlecht, George C. Verghese, Principles of Power Electronics, Reading Mass.: Addison-Wesley Publishing Company, 1991, Chapter 20.

[15] National Electrical Code 1993, Quincy, Mass.: National Fire Protection Association, 1992, Chapters 3 and 4.

[16] Stephen D. Goad, Theory and Design of Switched Mode Power Transformers for Minimum Conductor Loss, Ph.D. Dissertation, Virginia Polytechnic Institute and State University, December 1985.

[17] Herbert P. Neff Jr., Basic Electromagnetic Fields, New York: Harper and Row, 1981, pp. 111-114, 193-200.

VITA

Isaac Lynnwood Flory IV was born May 7, 1962, in Chattanooga, Tennessee.

He received his Bachelor of Science in Electrical Engineering from Virginia Polytechnic Institute and State University in December 1984. Upon graduating he became a Development Engineer for Hubbell Lighting Incorporated in Christiansburg, Virginia, working in the areas of discharge lighting ballasting and control. Isaac began taking graduate courses in electrical engineering in 1985, resigned in 1986, and resumed his part-time studies in 1989. He has continued his employment with Hubbell Lighting as a Senior Development Engineer while completing his M.S. degree requirements.

Isaac Lynnwood Flory IV